AD-A093 381 CALIFORNIA UNIV BERKELEY ELECTRONICS RESEARCH LAB F/G 20/9
PLASMA THEORY AND SIMULATION.(U)
JUN 80 C K BIRDSALL N00014-77-C-0578
UNCLASSIFIED NL

END
DATE FILMED
1-81
DTIC

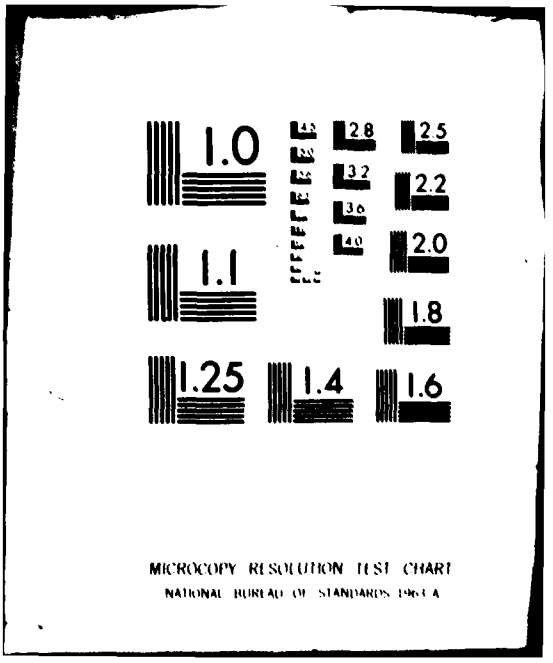
1.0
1.1
1.25
1.4
1.6
2.8
3.2
3.6
4.0
2.5
2.2
2.0
1.8
MICROCOPY RESOLUTION TEST CHART
NATIONAL BUREAU OF STANDARDS 1963-A

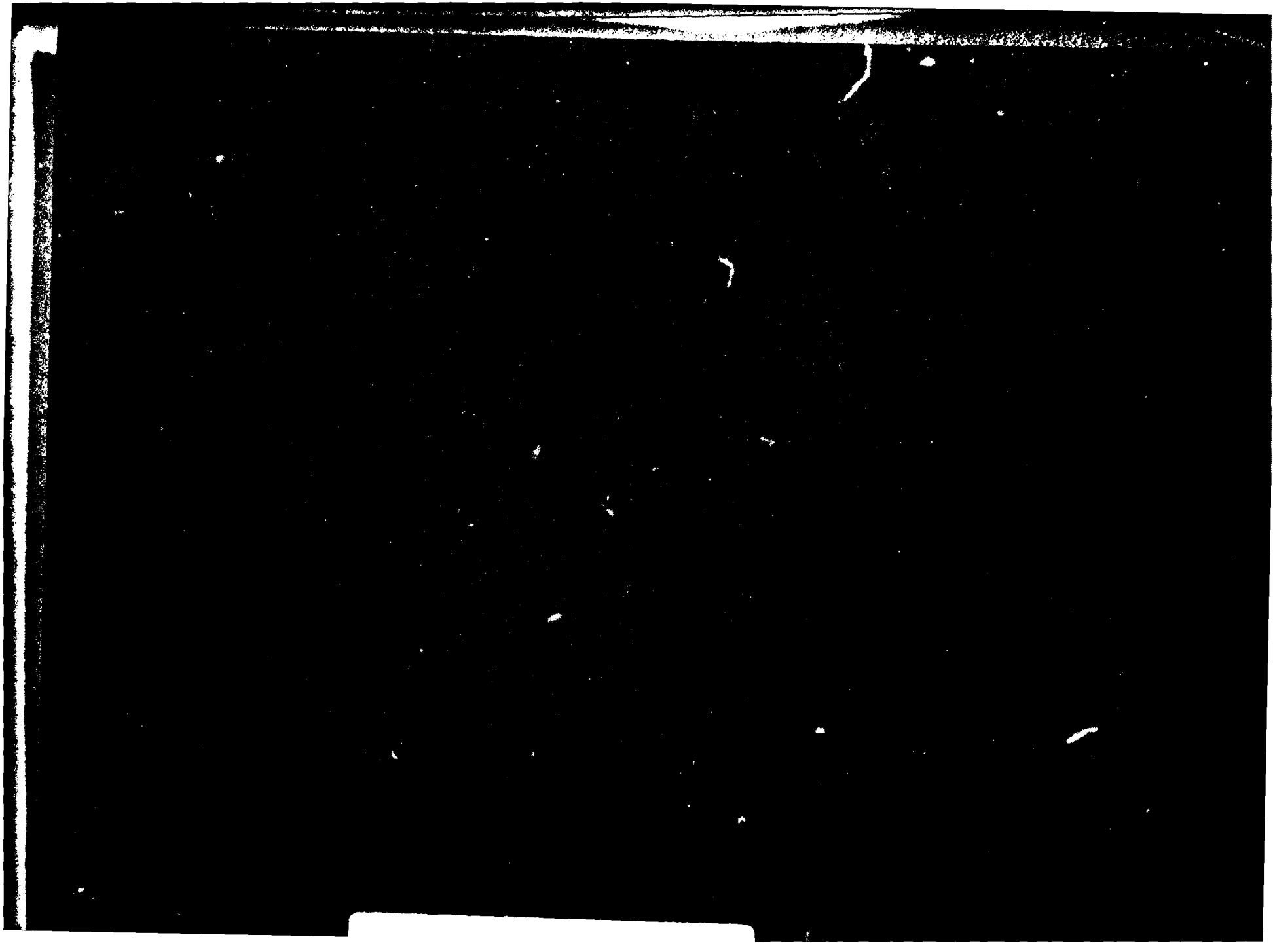

Plasma Theory & Simulation Group
DOE Contract No. DE-AS03-76F00034-DE-AT03-76ET53064
ONR Contract No. N00014-77-C-0578

ELECTRONICS RESEARCH LABORATORY
University of California
Berkeley CA 94720

SUMMARY OF PROGRESS FOR SECOND QUARTER — 1980

This is a summary of highlights of progress made by our group, for use by DOE and ONR contractors. The details appear in our Quarterly Progress Report.

LOWER HYBRID DRIFT INSTABILITY SIMULATIONS IN 2D USING EZOHAR. Our study of the lower hybrid drift instability has been expanded to 2d, to consider nonlocal effects and diffusion phenomena. Our earlier 1d work modeled electrons using a linear susceptibility; the present approach uses fully nonlinear particle electrons. Ions are still assumed to be unmagnetized. Initialization algorithms are developed, and some test runs are described.

MAGNETIZED MULTI-RING INSTABILITIES. Instabilities in simulation plasmas arise from the loading of particles onto "spokes and wheels" in velocity space, a technique which is commonly used to reduce noise. Maxwellian distributions may be constructed from (1) N equally weighted rings and (2) N uniformly spaced rings. Threshold values of ω_{pi}/ω_{ci} are given for 1, for Maxwellian envelope.

NONLINEAR QUASINEUTRAL SIMULATIONS OF FIELD-REVERSED PLASMAS. This 2d code is now working well, and has been applied to field reversed ion layers. Unstable modes with $m = 2,3,4$, and 5 have been observed, through the end of exponential growth.

FLUCTUATIONS AND LANDAU DAMPING. Thermal fluctuations in a simulation plasma and the associated resonance broadening and Landau damping were worked out and compared with simulations.

MULTI-BEAMING INSTABILITIES. A theory for the multi-beam instability associated with quiet start simulations of the lower hybrid drift was made.

ELECTROSTATIC SHOCKS IN THE AURORAL MAGNETOSPHERE. This is a guest contribution from colleagues at the Space Sciences Laboratory (whom we helped get started) describing particle simulations relevant to the observations of electrostatic shocks or double layers in the auroral magnetosphere on the S3-3 satellite. The simulations are both 1d1v and 1d3v (magnetized).

LINEARIZED 3D HYBRID SIMULATIONS OF FIELD-REVERSED SYSTEMS. The RINGHYBRID code has been applied to exponential rigid rotor equilibria, using a scheme whereby the coherent part of the perturbation is periodically reconstructed and the random part discarded, so that stochastic-orbit effects are suppressed.

Our group currently consists of five Ph.D. students, programmer ($\frac{1}{2}$), engineering aid ($\frac{1}{2}$), and ourselves. We presented two papers at the Sherwood Fusion Theory Meeting April 23-25 at Tucson, AZ. We presented four papers at the Ninth Conference on Numerical Simulation of Plasmas June 30-July 2 at Northwestern University, Evanston, IL. One journal article appeared. M. J. Gerver, from MIT, was a visitor for a week. ONR Contract renewal proposal was mailed April 24.

Alex Friedman
Post Doc

Charles K. (Ned) Birdsall
Professor, Principal Investigator

(9) Quarterly progress rept. no. 2 / 1 Apr - 30 Jun 80 (11) 30 Jun 80 (1)

SECOND QUARTER PROGRESS REPORT

on

(6) PLASMA THEORY AND SIMULATION. (12) 58

April 1 to June 30, 1980

Research during the Second Quarter of 1980 is reported here.

Our research group uses both theory and simulation as tools in order to increase the understanding of instabilities, heating, transport, and other phenomena in plasmas. We also work on the improvement of simulation, both theoretically and practically.

Our staff is (10)

Professor C. K. Birdsall *Principal Investigator*	191 M	Cory Hall	(642-4015)
Alex Friedman *Post Doctorate*	119 ME	Cory Hall	(642-3477)
Bruce Cohen, William Nevins *Lecturers, UCB; Physicists LLL*	L439 L439	LLL LLL	(422-9823) (422-7032)
William Fawley *Guest UCB; Physicist LLL*	L321	LLL	(422-9272)
Yu Jiuan Chen, Douglas Harned, Vincent Thomas, Niels Otani, Jin Soo Kim *Research Assistants*	119 MD	Cory Hall	(642-1297)
Stephen Au-Yeung *Programmer*	119 MD	Cory Hall	(642-1297)
Mike Hoagland *Research Typist*	119 M	Cory Hall	(642-7919)

June 30, 1980

(15)
DOE Contract AS03-76~~SF00034 DE-AT03-76ET53064~~
ONR Contract N00014-77-C-0578
DOE-DE-AS03-76SF00034

ELECTRONICS RESEARCH LABORATORY

College of Engineering
University of California, Berkeley
94720

12755 9

TABLE OF CONTENTS

*Indicates ONR supported areas.

**Guest Contributions

Section I
PLASMA THEORY AND SIMULATION

A. LOWER-HYBRID DRIFT INSTABILITY SIMULATIONS IN 2d USING EZOHAR

Yu-Jiuan Chen (Prof. C. K. Birdsall)

The study of the lower-hybrid drift instability has been expanded from one dimensional simulation using a hybrid ES1 code to two dimensional simulation which allows us to study the nonlocal effects and the diffusion phenomena using the EZOHAR code.

Similar to the one dimensional simulation, a slab shape is assumed and the equilibria are functions of x only. The drift velocity is in the y direction and the magnetic field is in the z direction. The simulations are carried out in the x-y plane. In our previous one dimensional simulations, ions were treated as fully nonlinear particles and electrons only appeared in a linear electron susceptibility. Now both ions and electrons are fully nonlinear particles; therefore, all the electron nonlinearities can be studied. We still restrict our simulation to a zero-beta plasma.

(1) Equilibrium

Since the mode frequency of the lower-hybrid drift instability is much higher than the ion cyclotron frequency, the ions are assumed to be unmagnetized. The ion pressure force is balanced by the ambipolar electric force in the equilibrium. From the Vlasov equation, the ion distribution function is then only a function of energy H_i where

$$H_i = m_i v^2/2 + e\phi(x) \ . \qquad (1)$$

Let the ion distribution function $f_i(H_i)$ be exponential, as

$$f_i(H_i) = C_i \exp\left(-\frac{\frac{1}{2}m_i v^2 + e\phi(x)}{T_i}\right) . \tag{2}$$

Rewrite Eq. (2) as a product,

$$f_i(H_i) = n_i(x) g_i(v) . \tag{3}$$

Here

$$g_i(v) = C_i \exp\left(-m_i v^2/2T_i\right) \tag{4}$$

is the Maxwellian distribution. The ion density profile is

$$n_i(x) = n_o \exp\left(-e\,\frac{\phi(x) - \phi(0)}{T_i}\right) . \tag{5}$$

n_o is the ion density at $x = 0$.

Similarly, the electron equilibrium distribution function is a function of two electron invariants: energy,

$$H_e = m_e v^2/2 - e\phi(x) \tag{6}$$

and the guiding center position

$$X = x - v_y/\omega_{ce} . \tag{7}$$

Let the electron distribution function $f_e(H_e, X)$ be given as

$$f_e(H_e, X) = F(X) \exp\left(-\frac{m_e v^2 - e\phi}{T_e}\right) . \tag{8}$$

For a small electron gyroradius and a slowly varying ambipolar field, i.e., $a_e \frac{d\phi}{dx}/\phi \ll 1$, the electric potential can be expanded around the guiding center

position as

$$\phi(x) = \phi(X) + \Delta x \left.\frac{d\phi}{dx}\right|_X + \ldots \tag{9}$$

where

$$\Delta x = x - X = v_y/\omega_{ce} \tag{10}$$

is the electron displacement from its guiding center. Therefore, Eq. (9) becomes

$$\phi(x) = \phi(X) - v_y E(X)/\omega_{ce} \, . \tag{11}$$

Substitute Eq. (11) into Eq. (8) and rewrite Eq. (8) as

$$f_e(H_e,X) = F(X) \exp\left(+ \frac{m_e v_E^2(X) + e\phi(X)}{2T_e} - \frac{m_e}{2T_e}\left\{v_x^2 + [v_y + v_E(X)]^2\right\}\right)$$

$$= N_e(X)\, g_e(v) \tag{12}$$

where $N_e(X)$ is the electron guiding center density profile and

$$g_e(v) = C_e \exp\left(- \frac{m_e}{2T_e}\left\{v_x^2 + [v_y + v_E(X)]^2\right\}\right) \tag{13}$$

is the electron drifting Maxwellian distribution.

From the Poisson equation,

$$\frac{dE(x)}{dx} = 4\pi e[n_i(x) - n_e(x)] \, , \tag{14}$$

and Eq. (5), $n_i(x)$ and $n_e(x)$ can be determined by choosing an appropriate $E(x)$.

An example of an equilibrium is shown in Fig. 1 when the E field has the form

$$E(x) = -4E_o \tanh^2(x/L)\ \mathrm{sech}^2(x/L) \ . \qquad (15)$$

(2) Simulation

The subroutine PTCLESET of the code EZOHAR has been modified to allow particle velocities to be loaded directly from an input file named VEL. If the parameter IW = 1, PTCLESET will get the particle v_x values in order out of VEL and use the random Maxwellian loader for v_y. For IW = 2, PTCLESET reads v_y in order from VEL and randomly loads v_x in a Maxwellian distribution. When IW = 3, both vx and vy values are obtained from VEL. If IW = 4(default), the Maxwellian loader is used for both v_x and v_y.

In our LHDI simulations, all four options were tested when VEL was set for the quiet start Maxwellian distribution. Parameters used are: $N_x = 64$, $N_y = 32$, $N_e = N_i = 32768$, $m_i/m_e = 100$, $\omega_{pe}^2/\omega_{ce}^2 = 1$, $(v_E/v_{ti})_{max} = 0.9$ and $L/\lambda_i = 50$. Simulation results agree very well with the lower-hybrid drift instability linear local theory. The nonlinearity of the instability has been studied. Saturation levels of the wave were in fair agreement with that predicted by ion trapping. Detailed nonlinear results will be given in the next Quarterly Progress Report.

B. MAGNETIZED MULTI-RING INSTABILITES

Jin Soo Kim (Prof. C. K. Birdsall, Dr. B. I. Cohen)

The normalized distribution function for N rings is the sum of δ-functions:

$$f_o(v_\perp, v_\parallel) = \sum_{s=1}^{N} \frac{a_s}{2\pi v_{\perp s}} \delta(v_\perp - v_{\perp s})\ \delta(v_\parallel) \qquad (1)$$

where a_s is the weighting of the s^{th} ring with $\sum_{s=1}^{N} a_s = 1$. The projection

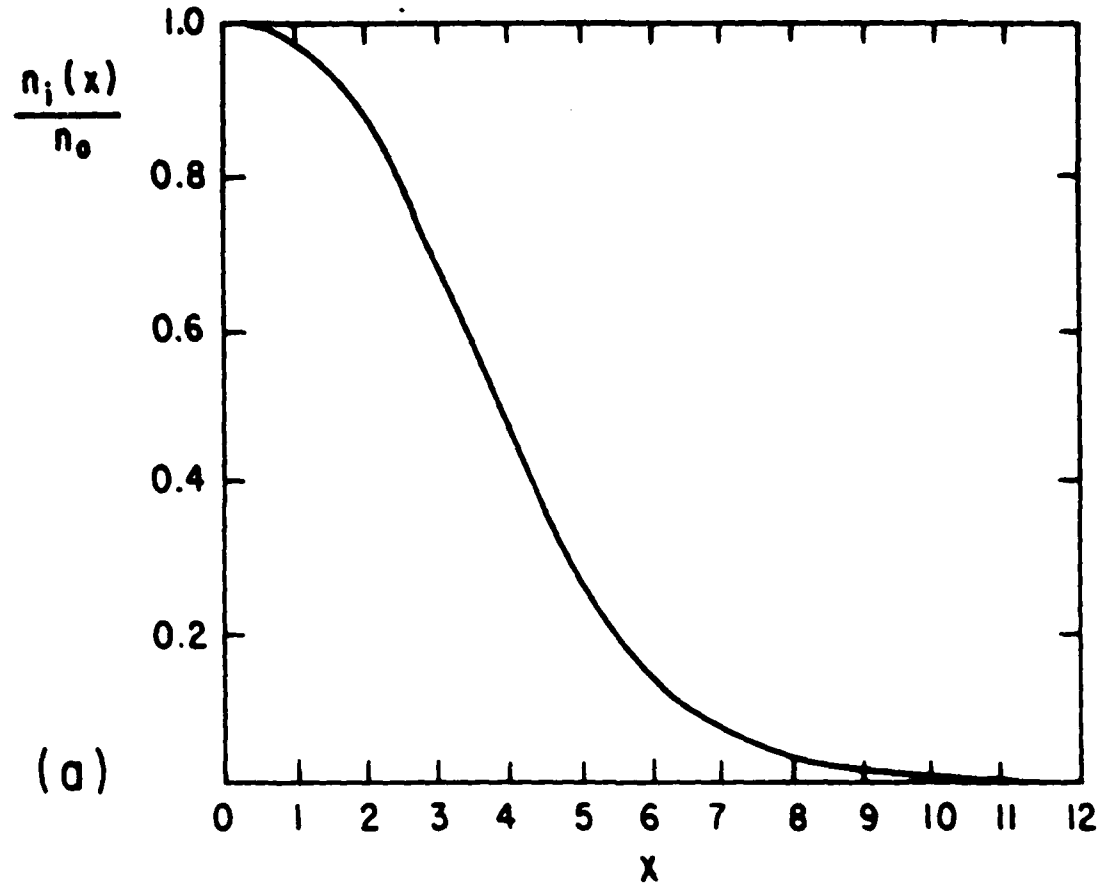

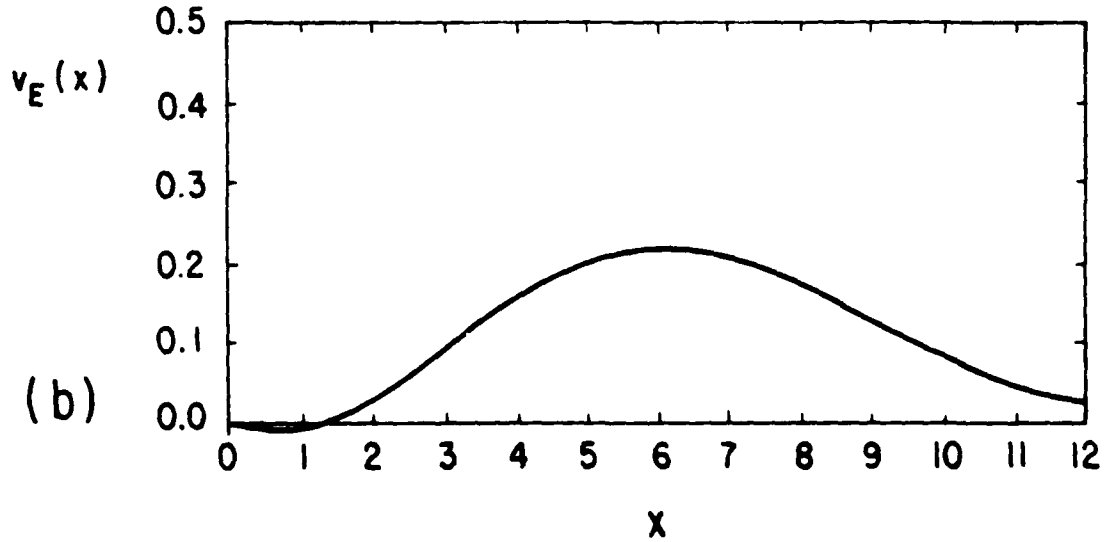

FIG. 1 Equilibrium profiles of (a) the normalized ion density $n_i(x)/n_o$ and (b) the relative electron-ion drift speed $v_E(x)/v_{ti}$. The difference between the ion and electron densities is too small to be seen in the figure.

of f_o on the v_x axis is

$$f_o(v_x) = \int f_o(v_\perp, v_\parallel)\, dv_y dv_\parallel$$

$$= \sum_{s=1}^{N} \frac{a_s}{\pi\sqrt{v_{\perp s}^2 - v_x^2}}\, \theta(v_{\perp s} - v_x) \qquad (2)$$

where $\theta(x)$ is a step function, equal to unity for positive argument and zero otherwise. This $f_o(v_x)$ is sketched in Fig. 1 for four equal density rings (without infinities).

The dispersion relations for one and N equal density ion rings were given in the previous QPR, for $k_\parallel = 0$. Adding cold background electrons, with each ring density reflected in its ω_{ps}^2 gives

$$D(\omega, k_\perp) = 1 + \frac{\omega_{pe}^2}{\Omega_e^2} - \sum_{s=1}^{N} \frac{\omega_{ps}^2}{\Omega_s^2} \sum_{\ell=-\infty}^{\infty} \frac{dJ_\ell^2(\mu_{\perp s})}{d\mu_{\perp s}} \frac{\ell\Omega_s}{\omega - \ell\Omega_s} \qquad (3)$$

where $\mu_{\perp s} = k_\perp v_{\perp s}/\Omega_s$ and J_ℓ is the Bessel function of the first kind of order ℓ. Adam Drobot in a private communication tells us to look for another term inside the sum, from relativistic theory, with denominator $(\omega - \ell\Omega_s)^2$, which may not be ignorable. We will look into this.

Typical roots of $D(\omega,k) = 0$ are shown in Fig. 2 for four unequal density rings, for total $(\omega_p/\Omega_c)_i^2 = 100$. This is incomplete, especially at $\omega_{LH} \approx \omega_{pi} = 10$, where some other behavior might be evident. Also needed is complex ω for one ring at the same total density, for comparison.

Mike Gerver (private communication) points out that we should probably always find instability at small $\omega/k_\perp$, inside the innermost ring. We see root a in Fig. 2 at $\mathrm{Re}\,\omega = 0$ (so-called zero frequency mode) and root h at $\mathrm{Re}\,\omega/k_\perp \approx 0.14 v_t$; if we went to larger k, we might see roots with phase

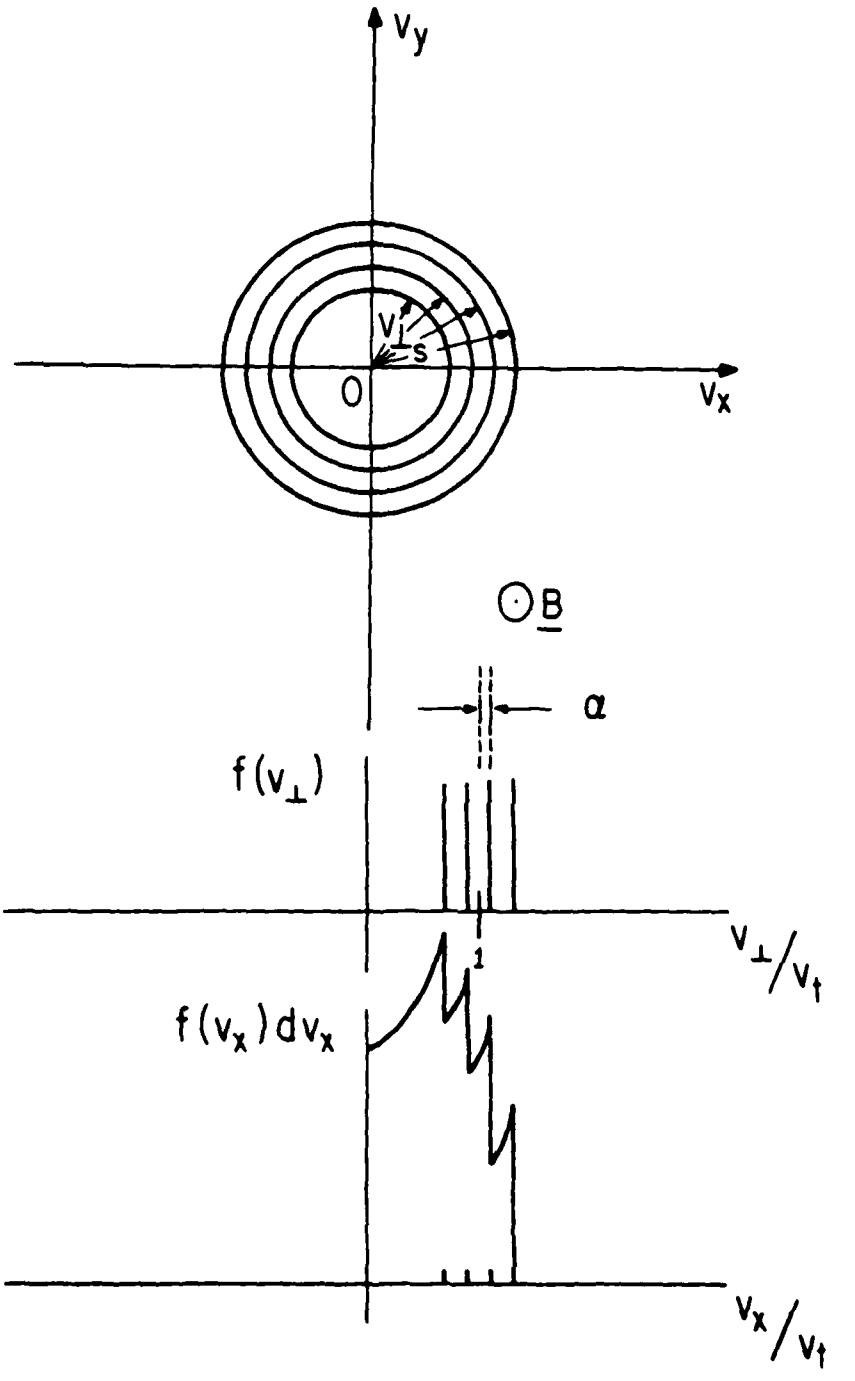

FIG. 1 $f_o(v_\perp)$ and $f_o(v_x)$ for four equal density rings.

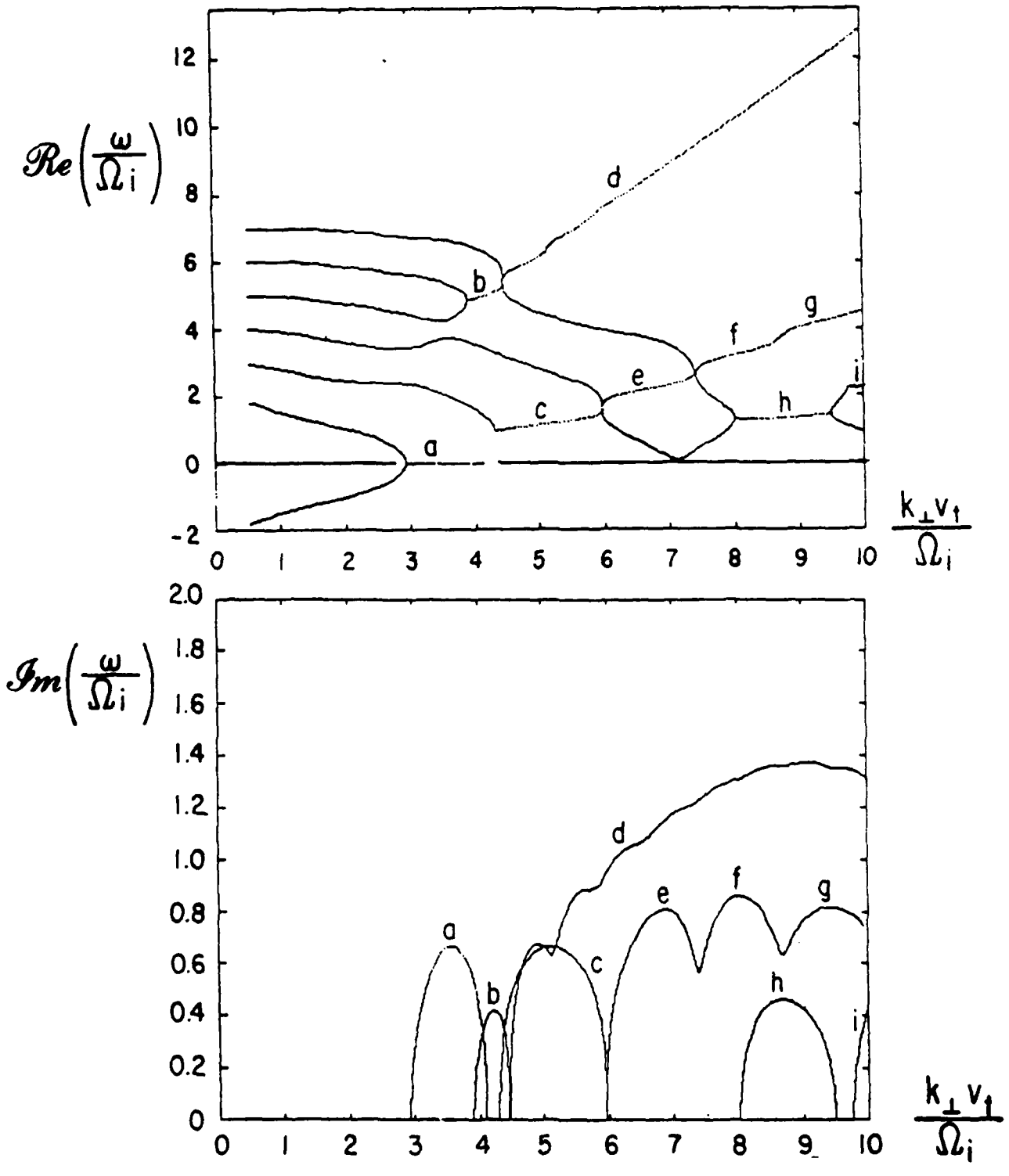

FIG. 2 Complex ω and real k are shown for four rings totaling $(\omega_p/\omega_c)_i^2 = 100$. Gyroradii are 0.875, 1.75, 2.63, 3.50 with $\omega_p^2 = 55.9$, 35.5, 7.85, and 0.718, respectively, and $\omega_{ci} = 1.0$. Ring velocities, relative to v_t, are 0.4 (roughly along branches c,e,f,g), 0.8, 1.2 (roughly along b,d) and 1.6.

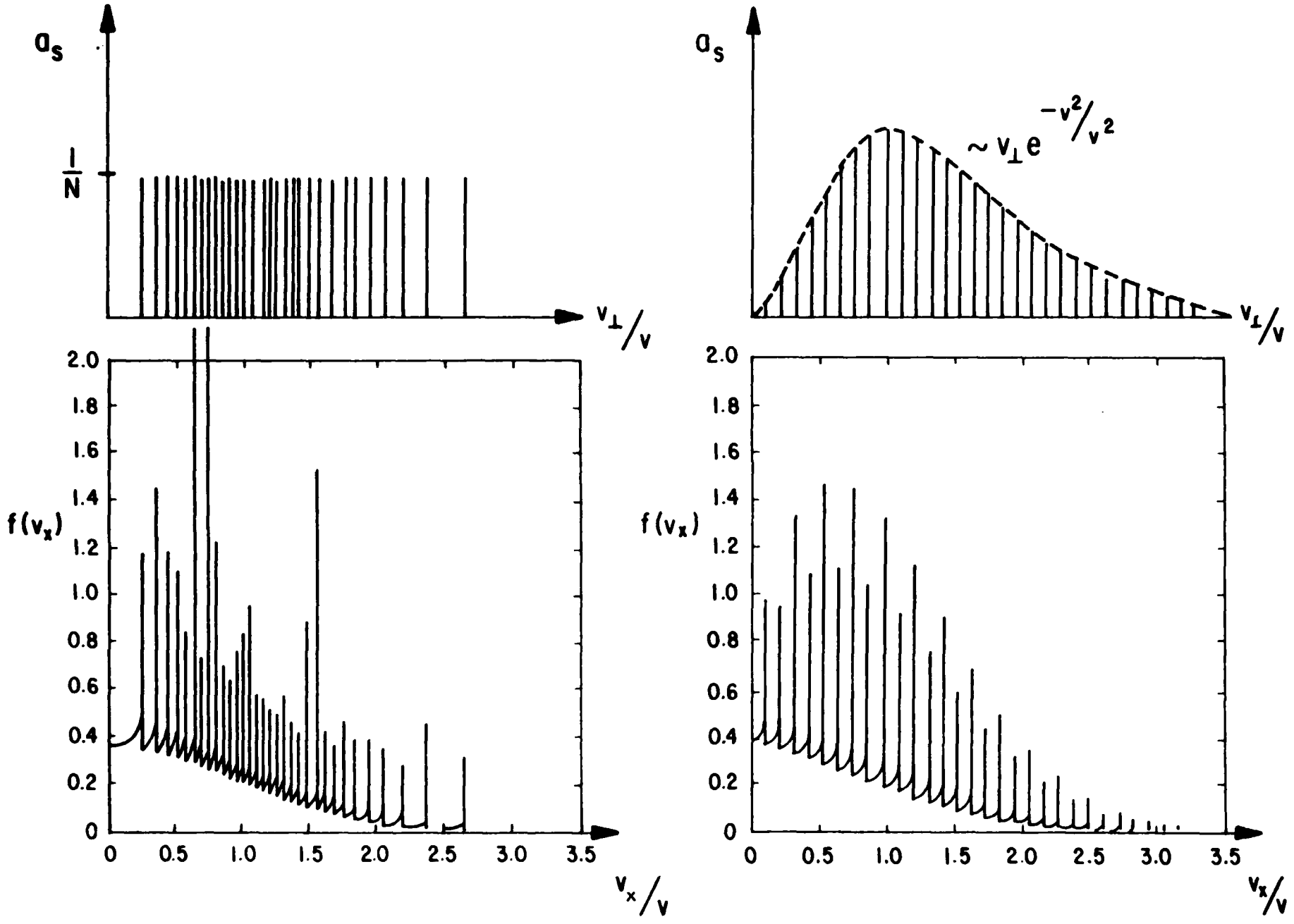

FIG. 3 Weights, a_s, and projected velocity distributions, $f(v_x)$ for Maxwellians (in $v_\perp$) for (a), equally weighted, unequally spaced rings and (b), unequally weighted, equally spaced rings.

velocities even smaller (than h). The slowest ring has $a_1 = 0.875$ and a_i (at v_t) is 2.19; hence, the ring velocities are radial lines of slopes 0.4, 0.8, 1.2, and 1.6.

We are extending this study to larger values of the parameters and to nonuniform envelopes of the rings, especially to Maxwellian; one object is to identify the number of rings needed for stability, a sore question in simulations. Two particular loadings of rings are being studied for simulating Maxwellians: (a) N equally weighted rings and (2) N uniformly spaced rings in velocity space, following the multi-beam studies of Gitomer and Adam.*

By choosing suitable $v_{\perp max}$ (say, $3.5v_{th}$) to assign values of $v_{\perp s} = \frac{s}{N} v_{\perp max}$, the weighting of rings is

$$a_s = v_{\perp s} e^{-v_{\perp s}^2/2v_{th}^2} \Big/ \sum_{s=1}^{N} v_{\perp s} e^{-v_{\perp s}^2/2v_{th}^2} \quad . \tag{3}$$

For the equally weighted case, we know that $a_1 = a_2 = \cdots = a_N = \frac{1}{N}$ and then the radii of rings ($v_{\perp s}$) in the velocity space are chosen by the following condition:

$$\frac{s}{N} = \int_0^{v_{\perp s}} e^{-v_\perp^2/2v_{th}^2} v_\perp \, dv_\perp \Big/ \int_0^{\infty} e^{-v_\perp^2/2v_{th}^2} v_\perp \, dv_\perp \quad . \tag{4}$$

The a_s and $f(v_x)$ are shown in Fig. 3 for both spacings.

*S. J. Gitomer and J. C. Adam, "Multibeam Instability in a Maxwellian Simulation Plasma", Phy. Fl. 19, pp. 719-722, May 1976.

The dispersion relations for the two models are:

$$D(\omega,k_\perp) = 0 = 1 + \frac{\omega_{pe}^2}{\Omega_e^2} - \frac{\omega_{pi}^2}{\Omega_i^2}\sum_{s=1}^{N}\sum_{\ell=-\infty}^{\infty}\frac{1}{\mu_{\perp s}}\frac{dJ_\ell^2(\mu_{\perp s})}{d\mu_{\perp s}}\frac{\ell\Omega_i}{\omega-\ell\Omega_i} \qquad (5)$$

$$D(\omega,k_\perp) = 0 = 1 + \frac{\omega_{pe}^2}{\Omega_e^2} - \sum_{s=1}^{N}\frac{\omega_{ps}^2}{\Omega_i^2}\sum_{\ell=-\infty}^{\infty}\frac{1}{(s\mu_{\perp 1})}\frac{dJ_\ell^2(s\mu_{\perp 1})}{d(s\mu_{\perp 1})}\frac{\ell\Omega_i}{\omega-\ell\Omega_i} \qquad (6)$$

in the presence of cold background electrons.

Primary interest in simulation is in knowing whether a Maxwellian envelope of N rings is stable or not, in order to choose N large enough in setting up initial thermal distribution. Hence, D = 0 of Eq. (5), equally weighted rings, was solved (by Niels Otani using Newton's method) up to the point (ω,k) of instability. The values of (ω,k) where the first complex roots occur are given in Fig. 4 in ω-k space with $(N,\omega_{pi}^2/\Omega_i^2)$ as parameters. In Fig. 5 the $(\omega_{pi}/\Omega_i)^2$ sufficient to make N rings unstable is shown. Note that use of Eq. (4) forces a $v_{\perp max}$; for examples, N = 32, $v_{\perp max} = 2.64v_t$ and N = 64, $v_{\perp max} = 2.89v_t$.

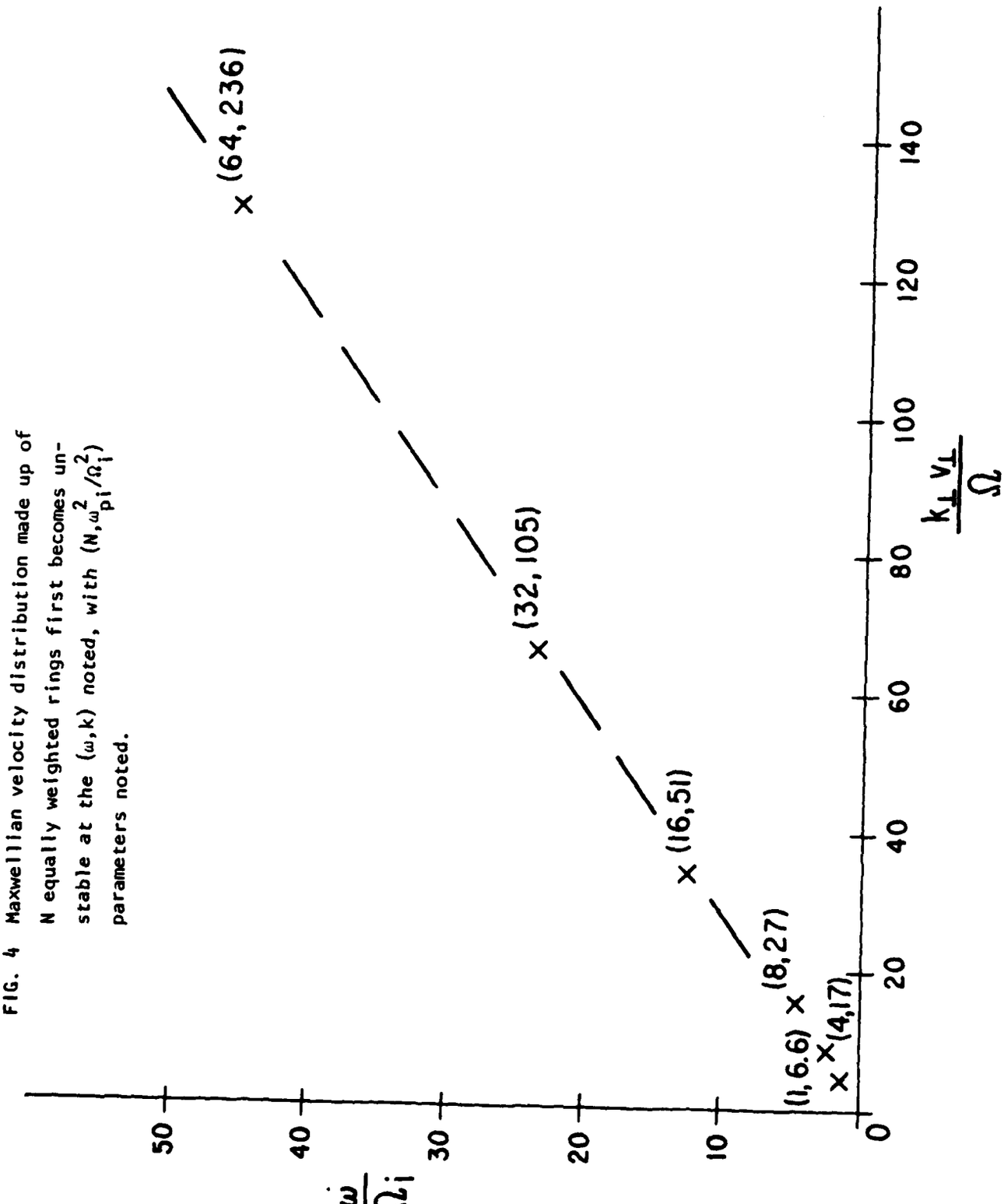

FIG. 4 Maxwellian velocity distribution made up of N equally weighted rings first becomes unstable at the (ω,k) noted, with $(N,\omega_{pi}^2/\Omega_i^2)$ parameters noted.

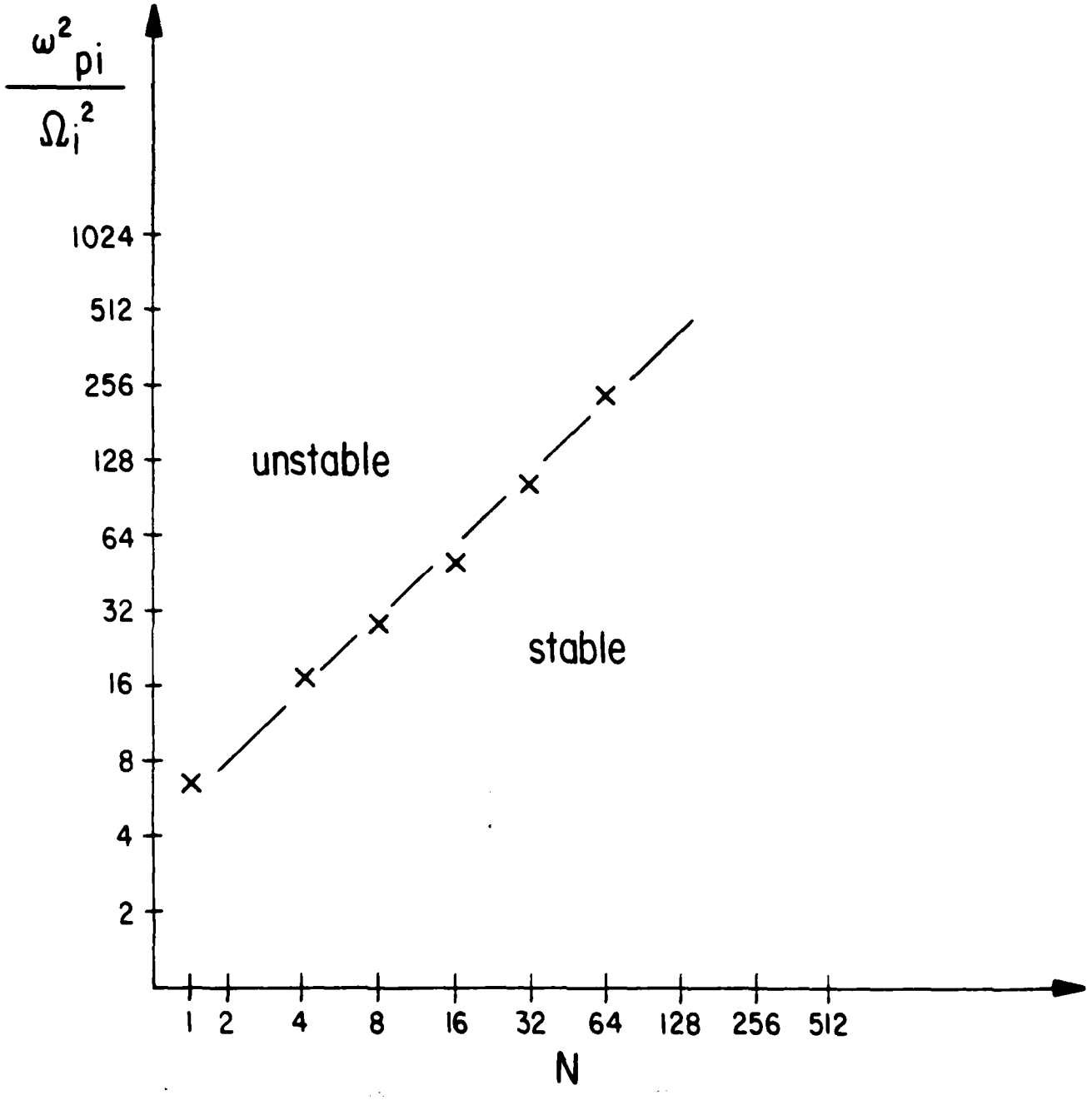

FIG. 5 Same distribution as in Fig. 4, with threshold value of ω_{pi}^2/Ω_i^2 given as a function of number of rings, N.

C. FIELD-REVERSED PLASMA SIMULATIONS, QUASINEUTRAL, IN 2d

Douglas Harned (Dr. Alex Friedman, Prof. C. K. Birdsall)

An equilibrium loader has been developed which produces rigid-rotor field-reversed equilibria. This loader has been used in conjuction with our two-dimensional quasineutral code, AQUARIUS. The code has been applied to field-reversed ion layers. Unstable $m = 2,3,4$, and 5 modes have been observed. For appropriate parameter ranges, the regions of instability have been found to correspond to those predicted by Lovelace.* A description of the equilibrium loader, as well as a complete discussion of ion-layer stability results, will appear in the next Quarterly Progress Report.

D. ORBIT AVERAGING

Vincent Thomas (Prof. C. K. Birdsall, Dr. B. I. Cohen)

Work is continuing in an effort to implement orbit averaging in a one dimensional electrostatic code, ES1. At the present time, the method appears to work when $\omega_{pe} < \omega_{ce}$ and $\underline{k} \cdot \underline{B} = 0$. An example was given in the previous QPR of the cold lower hybrid dispersion curve (including finite $k\Delta x$ corrections).

For the case $\omega_{pe} > \omega_{ce}$ (including the case $\omega_{ce} = 0$) no satisfactory results have been obtained. The simulation exhibits a violent instability in the first few time steps in which field quantities and kinetic energies typically increase by a factor of ~ 1000. The instability is saturated by trapping in the potential of mode 1 and is characterized by $\lambda_{De} \sim L$, the length of the system. This behavior is insensitive to $\omega_{pe}\Delta T$. All $\omega_{pe}\Delta T$ tried from the stability limit of the leapfrog algorithm to $\omega_{pe}\Delta T > 1000$ have been unstable.

*R. V. Lovelace, "Precession and Kink Motion of Long Astron Layers", Phys. of Fluids 22, No. 4, pp 708-717 (1979).

For $\omega_{pe}\Delta T \gtrsim 10$, the scheme requires taking microsteps for the ions as well as for the electrons so that $\omega_{pi}\Delta t_i$ never violates the leapfrog stability requirement for the microsteps.

A different method for biasing the equations of motion was presented by B. I. Cohen in the QPR in which the biasing is introduced by a backwards derivative of the velocity. This algorithm has been tried with orbit averaging. Similar behavior to simple orbit averaging was obtained, except when the biasing was very large (in the notation of the last QPR, $\varepsilon \lesssim 1$) so that all of the particles became frozen at equilibrium positions.

At the present time, we have developed no model which predicts the stability of the orbit averaging algorithm as functions of the parameters of the problem, particularly as ω_{ce}, ω_{pe} are changed.

E.* FLUCTUATIONS AND LANDAU DAMPING

Douglas Harned and Yu-Jiuan Chen (Prof. C. K. Birdsall)

(1) Theoretical Analysis of the Effect of Thermal Fluctuations

The spectral density of a warm plasma may be obtained from the fluctuation-dissipation theorem:

$$\frac{\langle E_L^2 \rangle (k,\omega)}{8\pi} = -\frac{T}{\omega} \operatorname{Im} \varepsilon^{-1}(\underline{k},\omega) \ . \qquad (1)$$

Here we have concerned ourselves with longitudinal fluctuations with $\underline{B} = 0$. The expression for $\varepsilon(\underline{k},\omega)$ is obtained from a Vlasov model

$$\varepsilon(\underline{k},\omega) = 1 + \sum_s \frac{1}{k^2\lambda_s^2} \sqrt{\frac{m_s}{2\pi T_s}} \int_{-\infty}^{\infty} dv_x \frac{kv_x}{kv_x - \omega - i\eta} \exp\left(\frac{-mv_x^2}{2T}\right) \qquad (2)$$

*This is material presented at our regular theory and simulation seminar on June 6, 1979, and considered to be of general and lasting interest, hence included here.

where the summation is over species. Considering a two-component, electron-ion plasma in thermal equilibrium (i.e., $T_e = T_i \Rightarrow \lambda_e = \lambda_i \equiv \lambda_o$, Maxwellian velocity distribution), ε becomes

$$\varepsilon(k,\omega) = 1 - \frac{1}{k^2\lambda_D^2}\left[W(Z_e) + W(Z_i)\right] \tag{3}$$

where $Z_s = \omega/\omega_{ps}k\lambda_D$ and $W(Z_s)$ is the Fried-Conte dispersion function. To substitute this into the fluctuation-dissipation theorem one uses the relationship

$$\text{Im}\,\varepsilon^{-1} = \frac{-\varepsilon''}{(\varepsilon')^2 + (\varepsilon'')^2} \tag{4}$$

where $\varepsilon \equiv \varepsilon' + i\varepsilon''$. Upon substitution we obtain

$$\frac{\langle E_L^2 \rangle (k,\omega)}{8\pi} = \tag{5}$$

$$-\frac{T}{\omega}\left\{\frac{\sqrt{\frac{\pi}{2}}\frac{\omega}{k^3\lambda_D^3}\left[\frac{1}{\omega_e}\exp\left(\frac{-\omega^2}{2\omega_e^2k^2\lambda_D^2}\right) + \frac{1}{\omega_i}\exp\left(\frac{-\omega^2}{2\omega_i^2k^2\lambda_D^2}\right)\right]}{\left[1 - \frac{1}{k^2\lambda_D^2}\text{Re}\left(W(Z_e) + W(Z_i)\right)\right]^2 + \frac{\pi\omega^2}{2k^6\lambda_D^6}\left[\frac{1}{\omega_e}\exp\left(\frac{-\omega^2}{2\omega_D^2k^2\lambda_D^2}\right) + \frac{1}{\omega_i}\exp\left(\frac{-\omega^2}{2\omega_i^2k^2\lambda_D^2}\right)\right]^2}\right\}$$

where the usual analysis has been used to obtain the imaginary part of the dispersion function, i.e.,

$$\text{Im}\,W(Z_s) = \frac{1}{k^2\lambda_D^2}\sqrt{\frac{\pi}{2}}\frac{\omega}{\omega_s k\lambda_D}\exp\left(\frac{-\omega^2}{2\omega_p^2k^2\lambda_D^2}\right).$$

Ordinarily the assumption is made that $k\lambda_D \ll 1$ so that Z becomes large in the

dispersion function. An asymptotic expansion can then be used to obtain the spectral density. However, here we will be interested in larger values of $k\lambda_D$ so that it will be possible to observe resonance broadening due to fluctuations as well as the associated Landau damping. In such a case (for $k\lambda_D \gtrsim .3$) the expansion technique is not valid.

The dispersion function may be written in the form:

$$W(Z) = 1 - Z \exp\left(\frac{-Z^2}{2}\right)\int_0^Z dy \exp\left(\frac{y^2}{2}\right) + i\sqrt{\frac{\pi}{2}}\, Z \exp\left(\frac{-Z}{2}\right). \quad (6)$$

A program SPECTRAL was written to evaluate numerically the integral in Eq. (6) and then to compute the spectral density for a given $k\lambda_D$ using Eq. (5). For large values of Z ($Z > 20$), the large argument expansion was used to evaluate W(Z). This program was used to provide theoretical curves (for $k\lambda_D$ from 0.1 to 1.0) for the spectral density for use in comparison with simulation values. The peak corresponds to ω_{real} and the width is a measure of ω_{imag}, the damping. We were interested in the values near $k\lambda_D = 0.4$ because these values seemed to be most amenable to simulation.

2. Simulation to Obtain Spectrum

The simulations were performed by loading a random Maxwellian velocity distribution of 8000 particles. $\lambda_D/\Delta x = 10$ was used. To obtain the spectral density, we used results from the post-processor ZED. We found that to obtain reasonable results it was necessary to use a large number of plasma periods (we used $\sim 300\tau_p$). For smaller numbers (e.g., 20) the finite time length of the run produced an inherent (minimum) line width that was larger than the resonance broadening due to Landau damping which we wanted to study, particularly for small $k\lambda_D$. Our results show that the resonance

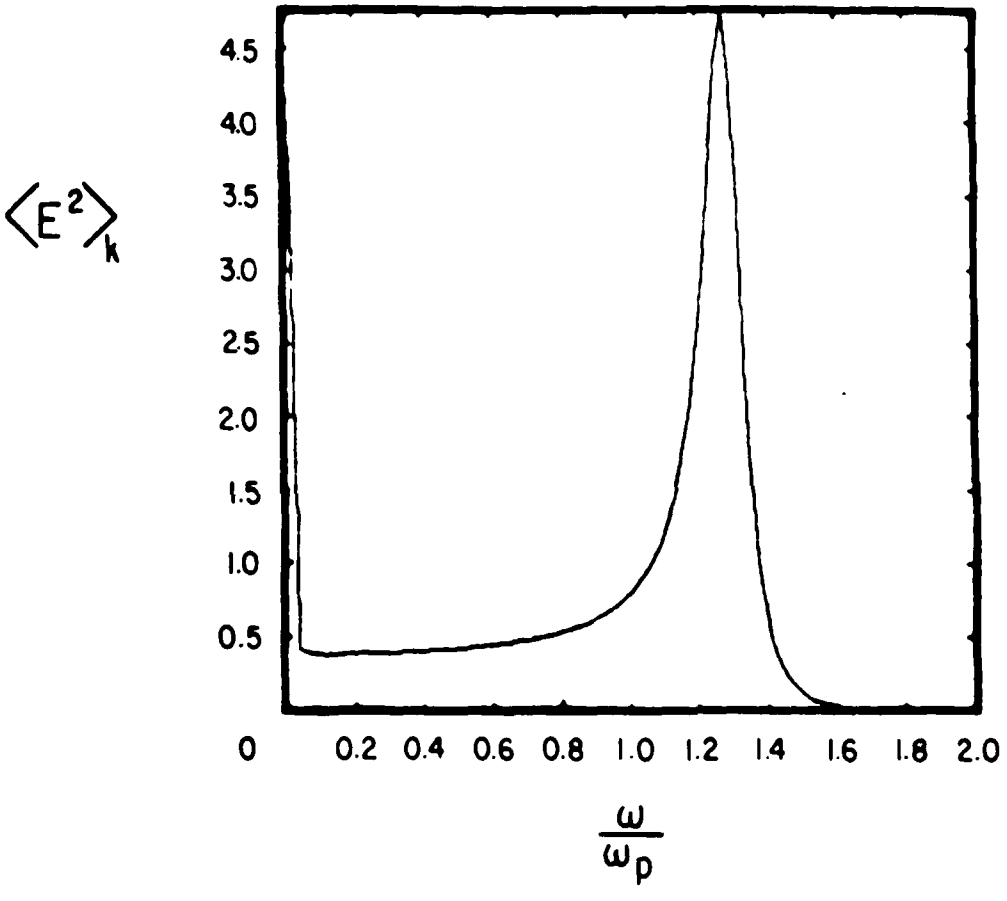

FIG. 1 Theoretical spectral density for $k\lambda_D = .4$, with the ion response included (near $\omega = 0$).

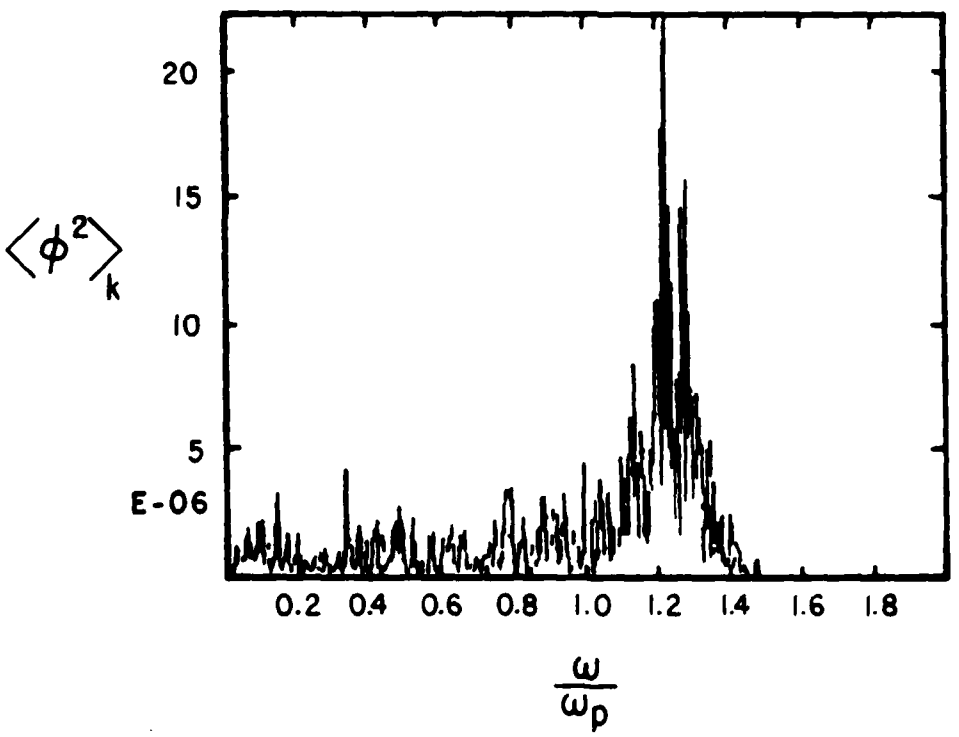

FIG. 2 Simulation result for spectral density, for $m_i \to \infty$ (no ion response), for $k\lambda_D = .4$, with about 300 plasma periods.

broadening seen in the simulations agreed fairly well with that predicted theoretically. Figures 1 and 2 show the theoretical and simulation spectral density plots for $k\lambda_D = 0.4$. The theoretical result shown includes the effect of the ions, while in our simulations, the ions were considered to be an infinitely massive neutralizing background. This is not a very important effect since ion fluctuations are negligible at frequencies as high as the plasma frequency. However, this is the reason for the low frequency peak in Fig. 1.

(3) Simulation of Landau Damping

Having obtained the fluctuation spectra, we then attempted to see Landau damping of a wave excited above the level of thermal noise. This requires a relatively large excitation since, for the number of particles ordinarily used in simulations, the noise level is high. However, with large excitations (at levels large enough to let particles cross) we were able to see evidence of Landau damping. The damping rate for $k\lambda_D \ll 1$ can be obtained by measuring the width of the Langmuir resonance and by direct measurement. Figure 3 shows the result for $k\lambda_D = 0.4$ and Fig. 4 shows the result for $k\lambda_D = 0.5$. The agreement between simulation and theory is good as shown in Table 1.

One concern was that for such large excitations, trapping effects could occur which might obscure the damping. In order for trapping to dominate over damping one should have $\omega_t > |\gamma|$ where γ is the damping rate and ω_t the trapping frequency, $\omega_t = k\sqrt{e\phi/m}$. For our simulations the trapping frequency and the damping rate were comparable at the initial level of excitation. However, this high level did not present a problem because after one oscillation, the wave had damped sufficiently to be out of the trapping regime.

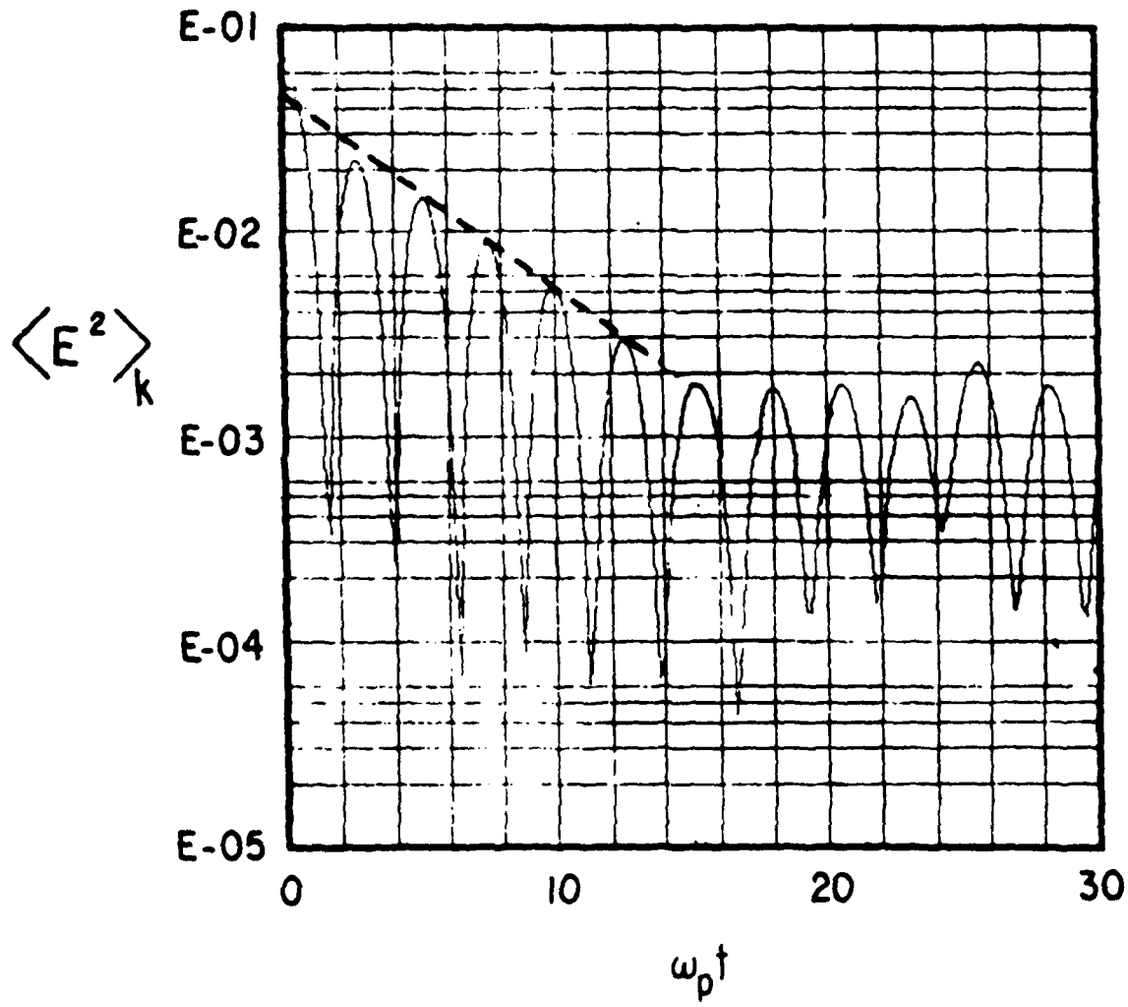

FIG. 3 Landau damping $k\lambda_D = .4$.

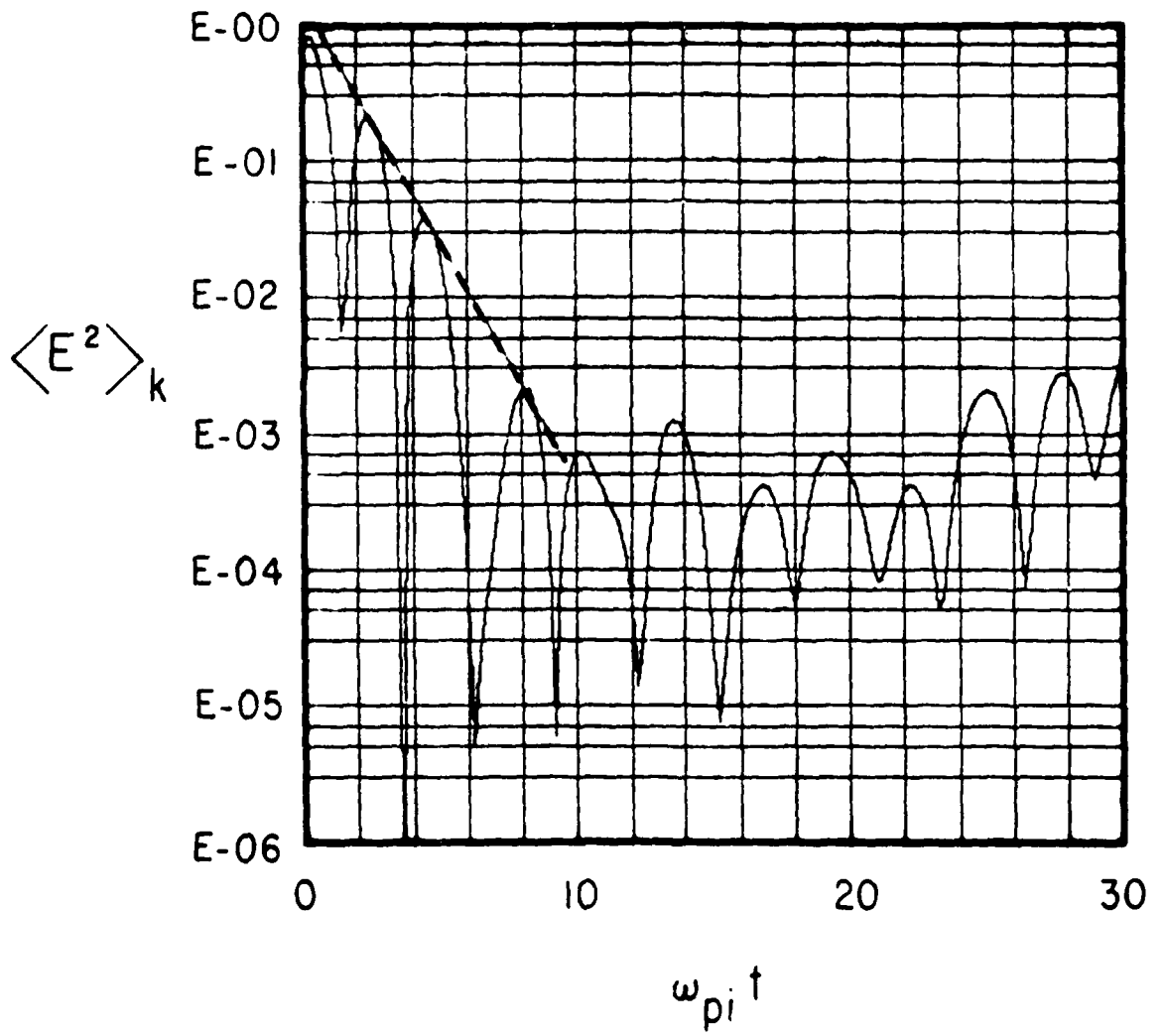

FIG. 4 Landau damping $k\lambda_D = .5$.

$k\lambda_D$	$\left(\frac{\omega}{\omega_e}\right)_{Th}$	$\left(\frac{\gamma}{\omega_e}\right)_{Th}$	From Comparison with Spectral Density Curves		From Direct Measurements of Damping
			$\left(\frac{\omega}{\omega_e}\right)_{sim}$	$\left(\frac{\gamma}{\omega_e}\right)_{sim}$	$\left(\frac{\gamma}{\omega_e}\right)_{sim}$
.3	1.16	.020	1.16	$\sim$.01	
.4	1.27	.108	1.24	$\sim$.13	.11
.5	1.37	.288	1.33	$\sim$.25	.31
.6	1.44	.548	$\sim$1.4	$\sim$.5	

Table I

Theoretical and simulation values for Langmuir frequencies and damping rates. The damping rates calculated from spectral density curves were obtained by measuring the width of the Langmuir resonance.

This is expected since any large amplitude wave that is constantly damped has particles changing from trapped to untrapped until the trapping effect becomes smallerthan the damping effect. In Fig. 3 trapping should only dominate during the first oscillation. This may account for the different initial slope.

(Langdon comments that the design for seeing Landau damping is

$$k\Delta v < kv_{trap} \equiv \omega_{trap} < \gamma_{Landau}$$

where v is the beam spacing.)

(The work reported herein is presented as interesting but not as exhaustive or complete.)

F. MULTI-BEAMING INSTABILITIES

Yu-Jiuan Chen (Prof. C. K. Birdsall)

Multi-beam instabilities, MBI, tend to plague attempts to make highly ordered, hence noiseless (quiet) initial conditions. Our last report on these problems was in QPR1, 1979, pp. 28, 29. However, they have continued to plague the LHDI work and have been observed and analyzed in our LHDI studies for the past two years; see especially QPR II, 1979, Fig. 1 on p. 5 for growth rates and Fig. 2 for LHDI growth plus multi-beam growth, with analyses in the text; see also QPR III, 1979, Fig. 2 on p. 4 for more mixed mode growth, and QPR IV, 1979, Figs. 2a,b on pp. 5,6 for similar growths.

This report provides theory for the MBI complementing that of Dawson* and Gitomer and Adam,** and was given as part of our plasma theory and simulation seminar June 5, 1979.

Any quiet start technique allows plasma instabilities of interest to be followed over many decades of growth from computer roundoff levels to saturation. However, the quiet start may not be useful for weakly unstable plasmas or for wave damping studies if it also produces the multibeam instability.

In ES1 code, there are two ways to initialize a Maxwellian velocity distribution, random or quiet. Here, we are interested in the quiet start method only. In this method, we first choose the number of beams NGR = N/NLG. NGR particles are uniformly distributed in x = (0,L/NLG) where L is the system length. A set of discrete velocities are found from the

---

*John M. Dawson, "Plasma Oscillations of a Large Number of Electron Beams", Phys. Rev. 118, No. 2, p. 381, 1960.

**S. J. Gitomer and J. C. Adam, "Multibeam Instability in a Maxwellian Simulation Plasma", Phys. Fl. 19, No. 5, p. 719, 1976.

cumulative probability density function

$$P(v) = \frac{\int_{-v_{max}}^{v} f(v')dv'}{\int_{-v_{max}}^{v_{max}} f(v')dv'} \qquad (1)$$

by selecting NGR values of P uniformly in the interval (0.,1.) and then finding which v(P) corresponds. For a Maxwellian, ES1 uses

$$v_{max} = 5v_{t2} \qquad (2)$$

$$f(v) = e^{-v^2/2v_{t2}^2} \qquad (3)$$

and

$$v_{t2} = \sqrt{T/m} \ . \qquad (4)$$

These particles' velocites are put into x space (L/NLG,L) and then scrambled in positions. All the particles have equal weights, but the beams set up using Eq. (1) are unequally spaced in velocity.

Following Dawson's paper, the linearized equations of motion for these beams are

$$\frac{\partial v_j}{\partial t} + V_j \frac{\partial v_j}{\partial x} = - \frac{eE}{m} \qquad (5)$$

$$\frac{\partial n_j}{\partial t} + N_j \frac{\partial v_j}{\partial x} + V_j \frac{\partial n_j}{\partial x} = 0 \qquad (6)$$

$$\frac{\partial E}{\partial x} = - 4\pi e \sum_j n_j \qquad (7)$$

where n_j and v_j are the perturbations in the density and velocity of the j^{th} beam while N_j and V_j are the corresponding unperturbed quantities. Assuming that solutions have the form $\exp[i(kx-\omega t)]$, Eqs. (5-7) can be re-written as

$$i(\omega-kV_j)v_j = -eE/m \tag{8}$$

$$(\omega-kV_j)n_j = kN_jv_j \tag{9}$$

$$ikE = 4\pi e\sum_j n_j \ . \tag{10}$$

From Eqs. (8-10) it is easy to obtain the well known dispersion relation,

$$1 = \frac{4\pi e^2}{m}\sum_{j=1}^{NGR}\frac{N_j}{(\omega - kV_j)^2} \qquad , \qquad N_j = NLG$$

$$= \frac{1}{NGR}\sum_{j=1}^{NGR}\frac{\omega_p^2}{(\omega - kV_j)^2} \tag{11}$$

Equation (11) was solved using SOLVER*, where the V_j are determined by Eq. (1). For NLG = 1 (meaning one particle per beam), $v_{tz} = 0.141421$, N = 4096, 8192 and 16384, the real part of the frequency of the most unstable mode (which is approximately kV_{NGR}, where V_{NGR} is the largest velocity, here taken to be $5v_t$), and the corresponding growth rate are plotted as a function of $k\lambda_D$ in Fig. 1. Although other unstable modes are not shown in Fig. 1, all of them have similar frequencies and growth rates. Figure 1 shows that the multibeam growth rate reduces by a factor of N at large k. The theore-

*H. Stephen Au-Yeung and Alex Friedman, "SOLVER: An Analytic Function Root Solving and Plotting Package", ERL Memo No. UCB/ERL M79/55, Aug. 31, 1979.

tical Langmuir dispersion curves are also shown in Fig. 1. As $0.3<k\lambda_D<0.6$ is the interesting region to study the Landau damping of Langmuir waves, Fig. 1 indicates that most of unstable multibeam frequencies are close to the Langmuir frequency, which makes it very difficult to excite only a Langmuir wave below the saturation level of the multibeam instability. A similar dispersion curve for N = 16384, NLG = 128, and $v_{t2} = 0.049$ was given by Gitomer and Adam.

G. ELECTROSTATIC SHOCKS IN THE AURORAL MAGNETOSPHERE

Mary K. Hudson and Douglas W. Potter (Space Sciences Laboratory, UC Berkeley, Guest Contributors)

In this section we summarize our recent plasma particle simulations relevant to the observations of electrostatic shocks or double layers in the auroral magnetosphere on the S3-3 satellite. First we review our one dimensional in space and velocity (1d1V), unmagnetized simulations for which we used an electrostatic particle code ES1 (Birdsall and Langdon, 1978). These simulations were useful for learning how to use the code and for checking that the results were consistent with theory, experiment, and previous simulations. We then modified the code to do 1d3V simulations in a magnetized plasma appropriate for the magnetosphere. Our initial results are reported here (Hudson and Potter, 1979).

Table I summarizes ours and other double layer simulations to date. Most previous work has been done with no magnetic field imposed. Our 1d3V simulations consist of infinite plane charge sheets at an angle $\pi/2 + \theta$ with respect to the magnetic field which is in the Z direction, as shown in Fig. 1; the simulation axis of charge sheet motion is along X. The charge sheets flow along B when an electric field or current is imposed in the Z

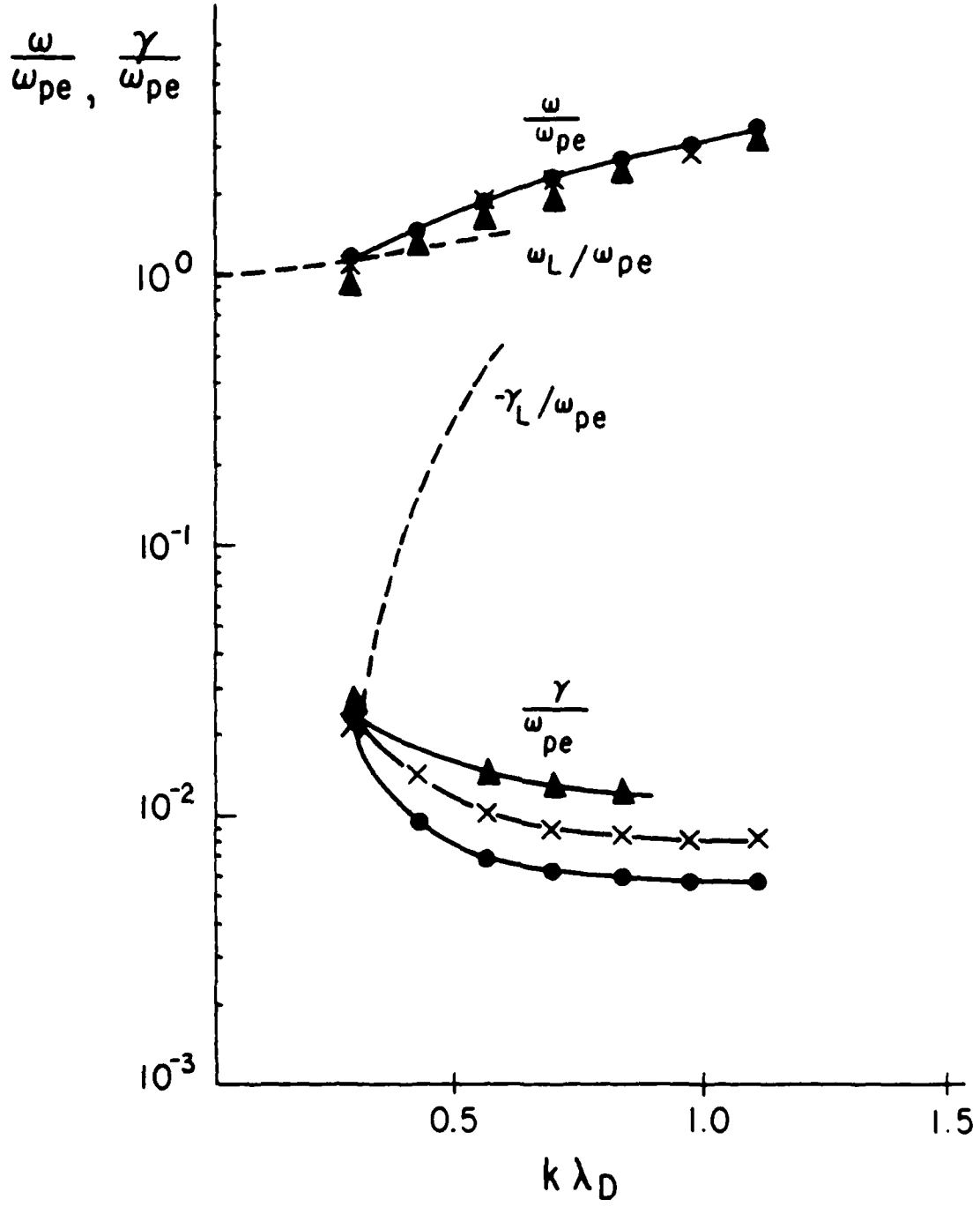

FIG. 1 Solutions for the most unstable mode multibeaming instability with $N = 4096(\Delta)$, $8192(x)$, and $16384(\bullet)$ beams. Sketched in are the Landau roots labelled L.

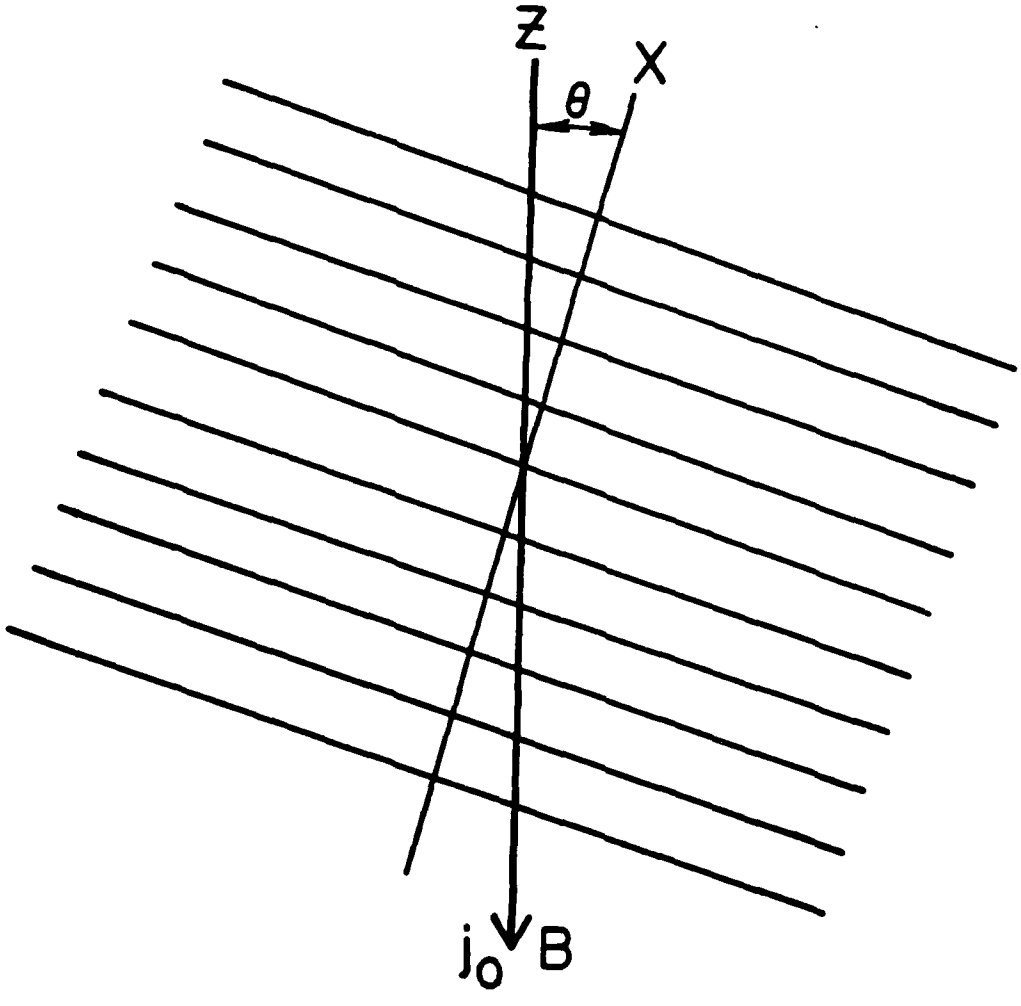

Figure 1

1d3V simulation geometry. Charge sheets are perpendicular to X and the magnetic field B is along Z.

Table I

	B	bc	E_o	j_o	D
Goertz & Joyce	0	np	0	$> A_e$	1d1V
Hubbard & Joyce	0	np	E_o	0	1d1V
de Groot et al.	0, B	p	0	$> A_e$	1,2d3V
Sato & Okuda	0	p	0	$< A_e$	1d1V
Hudson & Potter	0, B	p	E_o, 0	0	1d3V

direction, and the charge sheets oscillate about B at the electron and ion cyclotron frequency respectively. Thus, our simulation retains the dynamics of current flow along B and magnetized electrons and ions, while reducing the number of particles to be followed and the number of spatial grid points where fields are calculated cubicly from the three dimensional case.

Our initial runs were 1d1V with $B = 0$ and with periodic boundary conditions imposed. We chose an ion-to-electron mass ratio $M/m = 16$ and ion temperature $T_i = 0$, later changing to $M/m = 100$ and $T_i = T_e$, as described below. We imposed a constant electric field E_o greater than the runaway electric electric field which accelerates electrons to their thermal velocity in one collision time. We chose $E_o = .01$ in normalized computer units summarized in Table II. The electron charge-to-mass ratio was one, therefore the electron drift velocity $V = E_o t$ should have increased linearly with t such that $V = 1$ at $t = 100$ ($\omega_{pe} = 1$). The initial linear increase in electron drift velocity is apparent in Fig. 2.

Table II

Normalized Computer Units

	ω_{pe}	Ae	M/m	Ti/Te	t	n	Δx	Δt
1d1V	1	.25	16	0	50	81.9	.4	.2
1d3V	1	.25	100	1	128	32	.25	.2

L = system length
n = charge sheet density
Δx = space grid steps
Δt = time grid steps

However, the Buneman instability intervened by $t = 100$. The frequency and growth rate of the Buneman instability can be determined from the plot of fluctuating $\tilde{E}^2/8\pi$ vs. t in Fig. 3 ($\omega \approx .025$ and $\gamma = .2$ in units of $\omega_{pe} = 1$). The wavelength determined from plots of density fluctuations vs. X at fixed t is the order of $100\lambda_D$. These results are consistent with linear theory (Buneman, 1959).

The linear increase in electron drift with time is apparent in Fig. 2, up to the onset time of the Buneman instability. Current saturation and falloff at $t \sim 100$ is due to backscattering from fluctuations. This is evident in plots of the electron distribution function at fixed times. Figure 4a is a plot of the electron distribution function at $t = 80$. The freely accelerated electron Maxwellian peaks at $V = -.8$, consistent with $V = E_o t$, and there are few electrons near $V = 0$. Figure 4b shows a backscattered electron population at $t = 120$ responsible for the decrease in current in Fig. 2. E_o continues to accelerate the electron distribution function and turbulence continues to decelerate it. A freely accelerated electron population is apparent at $V = -2.$ at $t = 200$ and at $V = -5.$ at $t = 500$ in Figs. 4c and 4d.

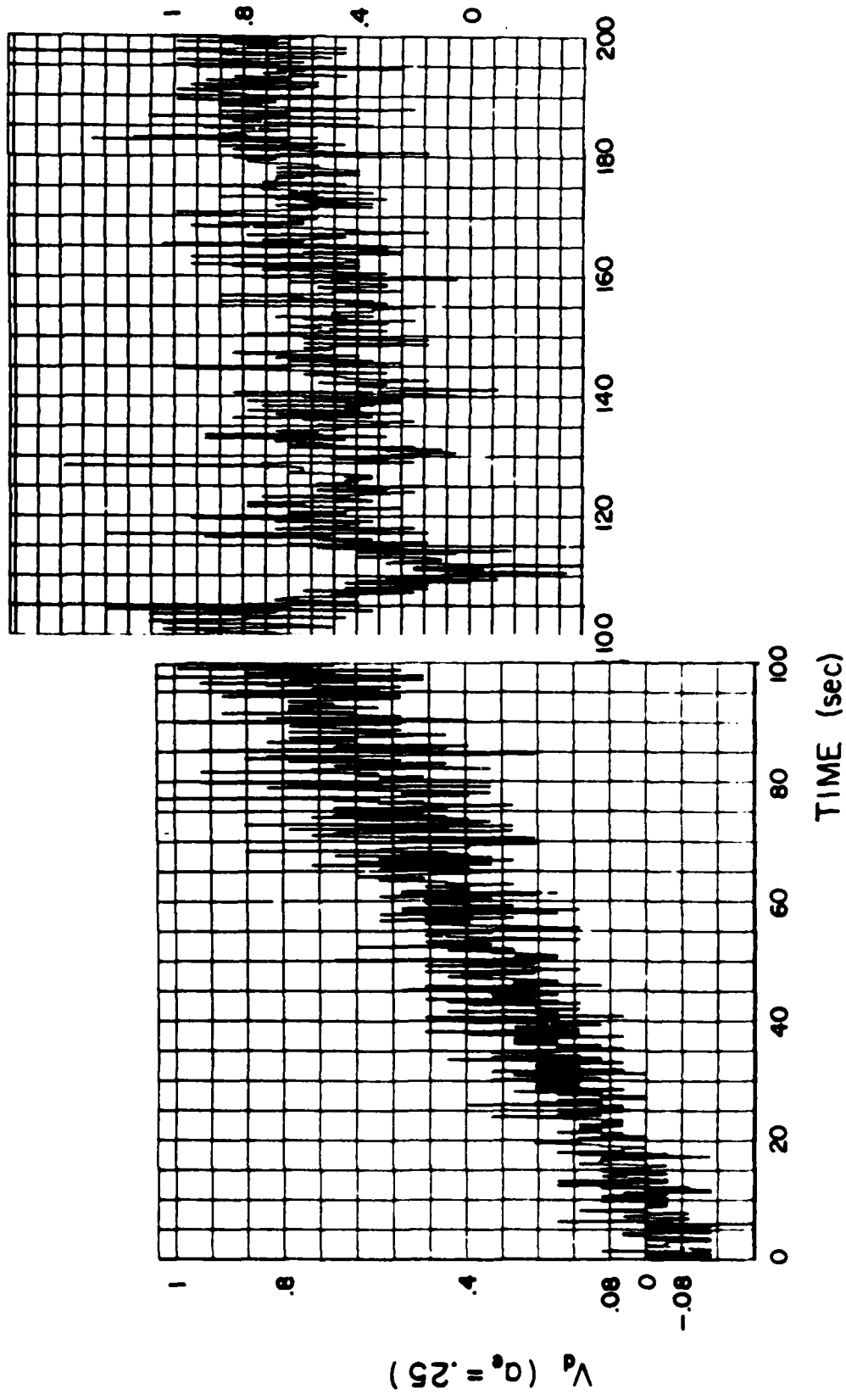

Figure 2

Plot of electron drift velocity vs. time in our 1d1V simulation.

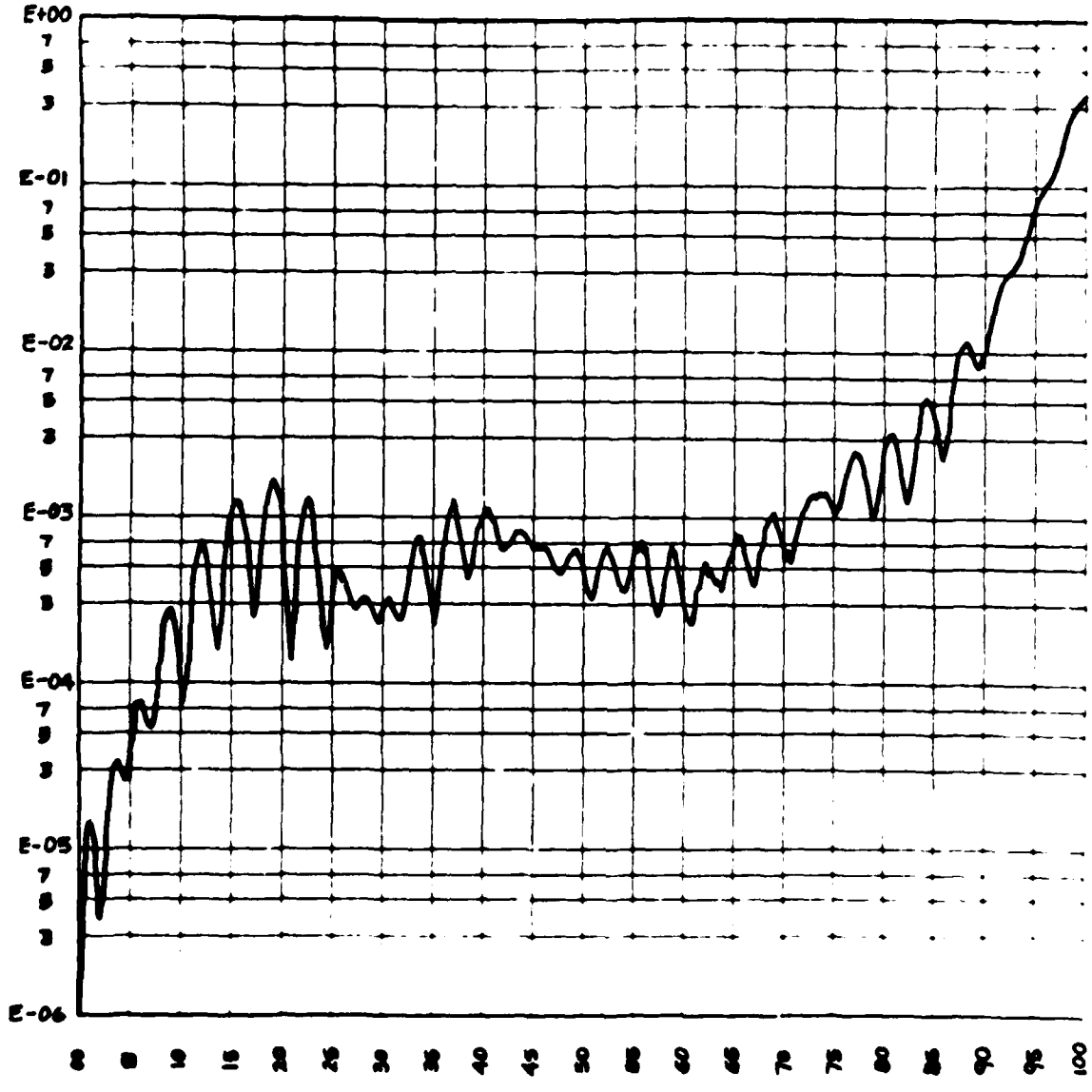

Figure 3

Plot of $\tilde{E}^2/8\pi$ vs. t from t = o to t = 100 ($\omega pe = 1$).

The continued increase in current at later times in Fig. 2 is due to a combination of current carried by runaways and the increase in the critical drift for instability $V_c \propto A_e$, the electron thermal speed. The latter is increasing due to turbulent heating of electrons and its increase is apparent in the velocity spread of the electron distribution in Fig. 4a-d. Thus the following scenario occurs: when $V_d > V_c$, instability develops which reduces V_d and increases $V_c \propto A_e$, thereby shutting off the instability. However, $V_d \propto E_o t$ increases again until $V_d > V_c$ and the cycle repeats. The oscillatory nature of the instability is apparent in Fig. 5, which is an extension of the plot of electric field fluctuations in Fig. 3 to later times. This oscillatory behavior has been reported in other simulations, cf. Davidson et al. (1970) and the review by Papadopoulos (1977).

In our 1d3V simulations, we have imposed an electric field along B with the simulation axis at an oblique angle $\theta = \pi/2 - .1$. The current behavior plotted in Fig. 6 is similar to the 1d1V case. This is a plot of $j_x = j_z \sin .1 \simeq .1 j_z$, and is therefore reduced by a factor of 10 from the 1d1V case for the same E_o. Note that Buneman saturation of current occurs slightly later than in the 1d1V case because ions are now warm ($T_i = T_e$ and $M/m = 100$ is assumed) and contribute Landau damping, which raises the threshold drift and increases time $t = V/E_o$ to achieve that drift.

We observe oscillating potential structures evolving by $t = 100\omega_{pe}^{-1}$ at Buneman wavelengths $\lambda = 85\lambda_D$ along X. This is the dominant mode thus far in our simulations because it has the fastest growth rate of any current driven electrostatic instability for currents above its threshold which are produced by the applied E_o. In the magnetospheric case of weaker currents other modes may prevail. We plan to simulate the effect of other current

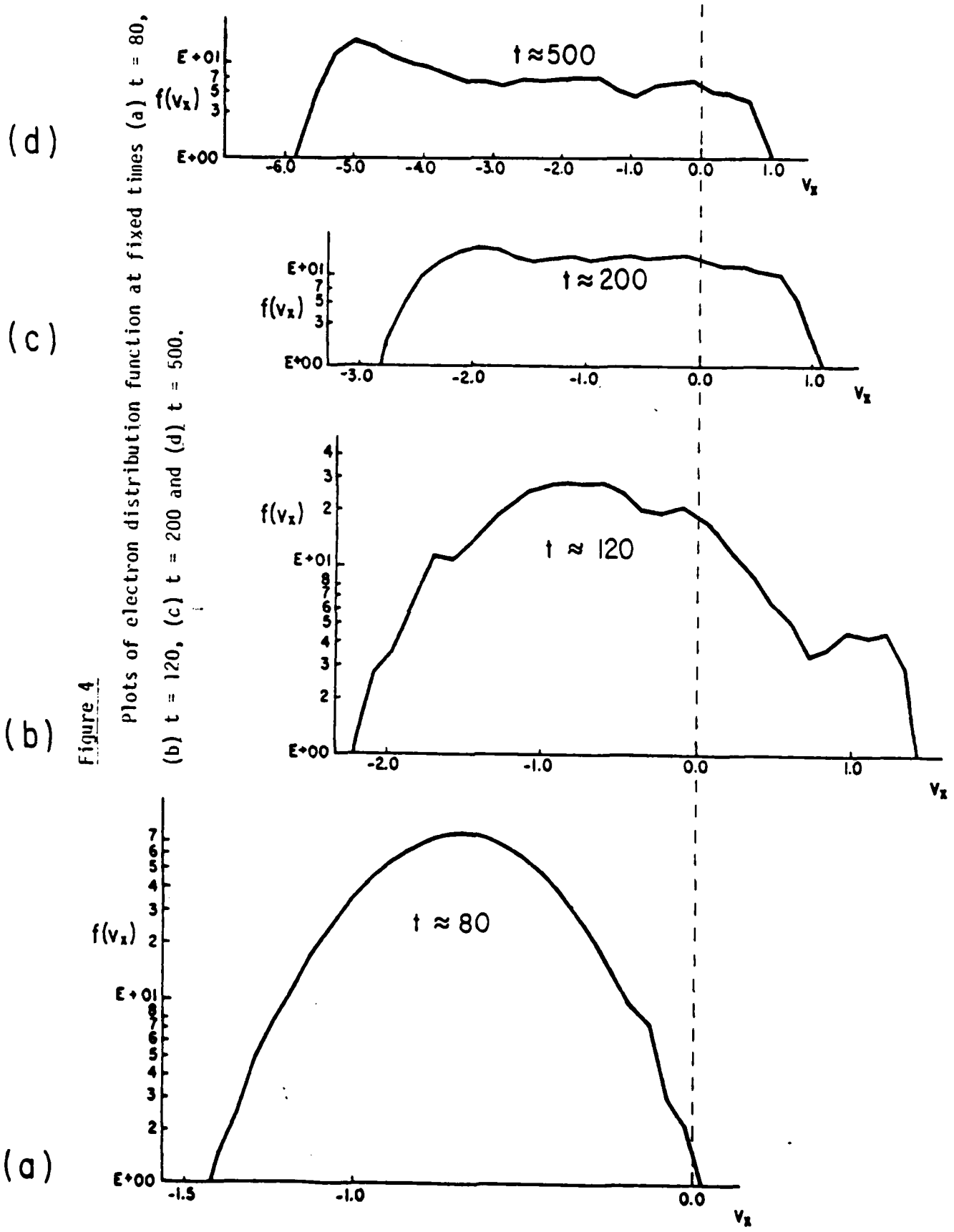

Figure 4

Plots of electron distribution function at fixed times (a) t = 80, (b) t = 120, (c) t = 200 and (d) t = 500.

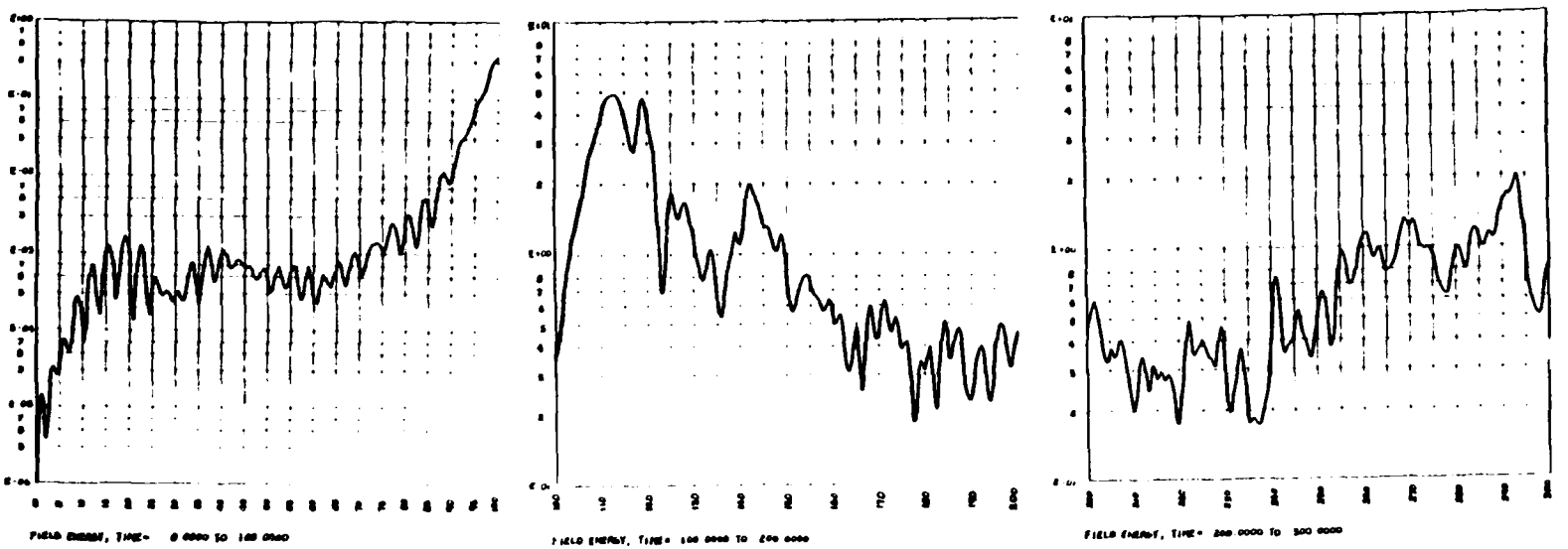

Figure 5

Plot of $\tilde{E}^2/8\pi$ vs. t from t = 0 to t = 300.

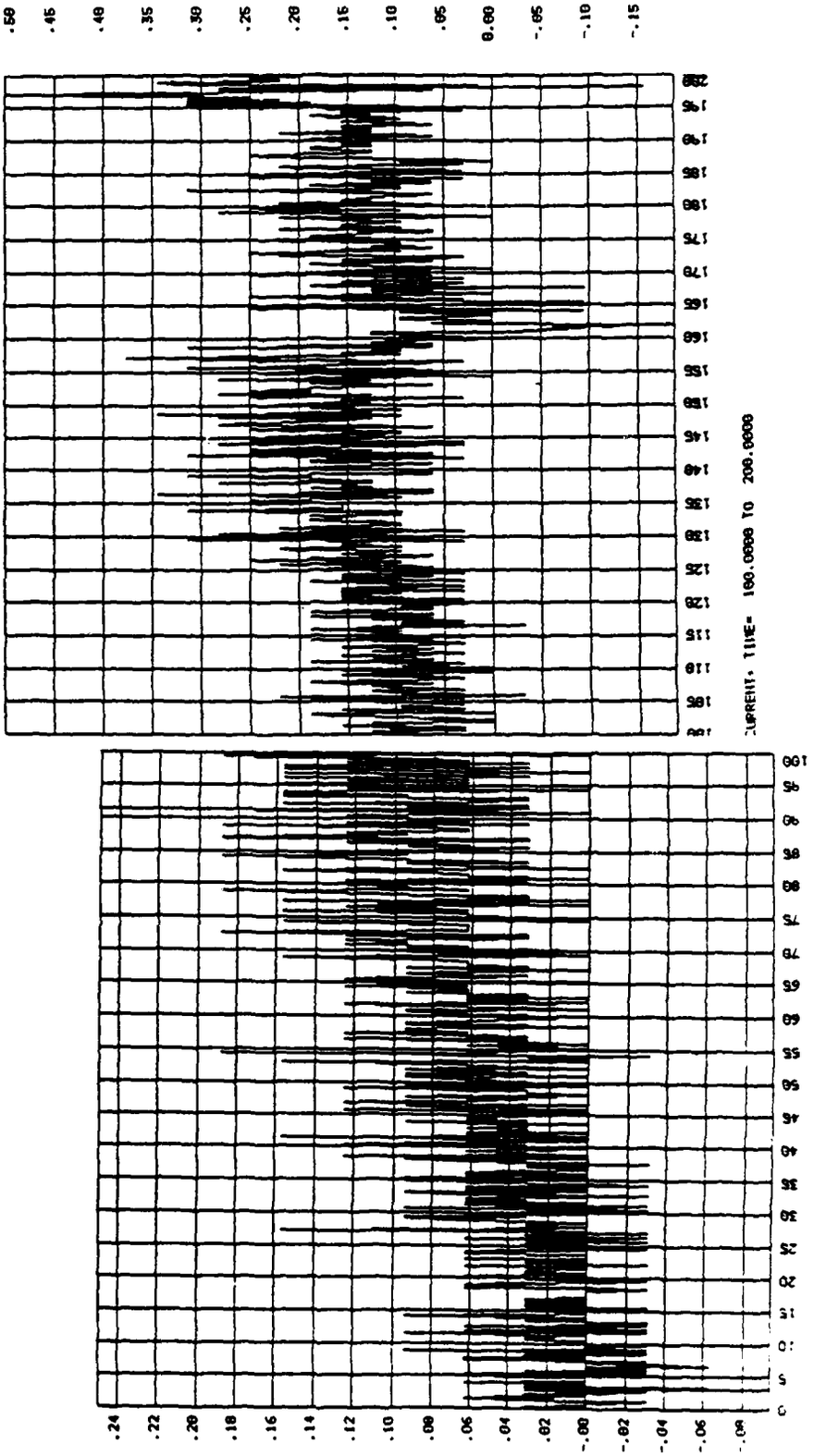

Figure 6

Plot of electron current vs. time in our 1d3V simulation.

driven modes by (1) applying a weaker electric field for a longer time to see if current saturation by instabilities with a lower current threshold, e.g., ion cyclotron or ion acoustic in the presence of electron heating, precludes excitation of the Buneman instability in the magnetized case; and (2) by applying a current below threshold for the Buneman instability.

We observe the coalescence of potential fluctuations into a single structure by $t = 600\omega_{pe}^{-1}$ in Fig. 7. In a 1d1V unmagnetized simulation with periodic boundary conditions Biskamp and Chodura (1973) have shown that a succession of wave bursts of the type evident in Fig. 5 each doubles the wavelength of the dominant mode by coalescence of BGK modes. The dominant mode asymptotically approaches the longest wavelength allowed by the size of the simulation system. Figure 7 gives the impression that if periodic boundary conditions were not imposed which force the potential to be the same on both sides, a single potential drop would exist across the system. The magnitude of $e\phi/T = 2.4 \times 10^3$ is enough to accelerate 1eV electrons to keV auroral energies. Note that this electric field structure is oblique to the magnetic field with a parallel component, analogous to the electrostatic shocks which have been observed on the S3-3 satellite (Mozer et al., 1977). We plan to reduce the applied current, change the boundary conditions from periodic to nonperiodic, and determine under what circumstances oblique shocks of the type commonly observed on S3-3 occur on auroral field lines, vs. one dimensional double layers, where the potential drop is strictly along B.

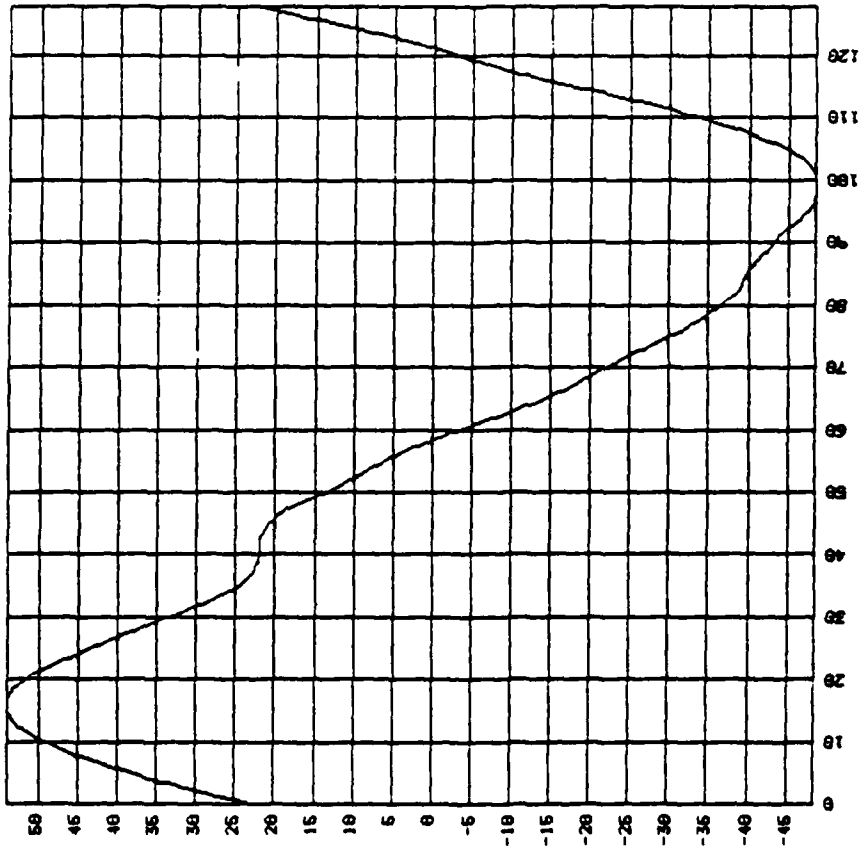

Figure 7

Electrostatic potential profile vs. X at t = 600.

References

Birdsall, C. K. and Langdon, A. B., Plasma Physics Via Computer Simulation, Vols. 1-4, EECS Dept. U.C. Berkeley, 1978.

Biskamp, D. and Chodura, R., "Collisionless Dissipation of a Cross-Field Electric Current", Phys. Fluids 16, 893, 1973.

Buneman, O., "Dissipation of Currents in Ionized Media", Phys. Rev. 115, 503, 1959.

Davidson, R. C., Krall, N. A., Papadopoulos, K. and Shanny, R., "Electron Heating by Electron-Ion Stream Instabilities", Phys. Rev. Lett. 24, 579, 1970.

Hudson, M. K. and Potter, D. W., "Particle Simulations of Electrostatic Shocks", Trans. Am Geophys. Union 60, 913, 1979b.

Mozer, F. S., Carlson, C. W., Hudson, M. K., Torbert, R. B., Parady, B., Yatteau, J., and Kelley, M. C., Phys. Rev. Lett. 38, 292, 1977.

Papadopoulos, K., "A Review of Anomalous Resistivity for the Ionosphere", Revs. Geophys. and Space Sci. 15, 113, 1977.

Goertz, D. K. and Joyce, G., "Numerical Simulation of the Plasma Double Layer", Astrophys. Space Sci. 32, 165, 1975.

Hubbard, R. F. and Joyce, G., "Simulation of Auroral Double Layers", J. Geophys. Res. 84, 4297, 1979.

deGroot, J. S., Barnes, C. Walstead, A. E., and Buneman, O., "Localized Structures and Anomalous dc Resistivity", Phys. Rev. Lett. 38, 1283, 1977.

Sato, T. and Okuda, H., "Ion Acoustic Double Layers", Phys. Rev. Lett. 44, 740, 1980.

Hudson, M. K. and Potter, D. W., "Particle Simulations of Electrostatic Shocks", Trans. Am. Geophys. Union 60, 913, 1979.

H. FIELD REVERSED EQUILIBRIA, INTRINSIC STOCHASTICITY, AND COLLECTIVE STABILITY

Alex Friedman

We have developed a computer program, RIGIDROTOR, to generate axisymmetric field reversed Vlasov equilibria for use with our linearized 3d hybrid simulation code RINGHYBRID[1]. In these equilibria the current is carried entirely by hot ions with gyroradii which may range from infinitesimal (as in the Hill vortex equilibria) to of order the system size (as in ion ring equilibria); charge neutrality is assumed. We describe the equilibrium calculation, the intrinsic stochasticity and hence local instability of particle orbits in these equilibria, the problem this instability presents for studies of collective behavior, and a means of partially overcoming the difficulty.

We assume an exponential rigid rotor equilibrium distribution function for the ions of the form

$$F = n_0(2\pi mT)^{-3/2}\, e^{-[(H - \Omega P_\theta)/T]}, \tag{1}$$

where $H = mv^2/2$ is the particle kinetic energy, $P_\theta = mrv_\theta + qrA/c$ is the canonical angular momentum, $A = A_\theta(r,z)$ is the azimuthal component of the vector potential, T is the temperature in energy units, and n_0 is the density on axis. The velocity distribution is Maxwellian in the rotating frame, and the mean azimuthal velocity is everywhere $r\Omega$. After integrating $v_\theta F$ over velocities, Ampere's law can be written:

$$(\nabla X \nabla X A\hat{\theta})_\theta = (4\pi/c)qr\Omega n_0 e^{[qr\Omega A/c + mr^2\Omega^2/2]/T}. \tag{2}$$

The algorithm used to solve this equation is similar to a new MHD equilibrium algorithm[2]. We introduce an r-z grid, and new parameters C_T and C_n such that

$$T = C_T\, \psi_{max}, \qquad n_0 = C_n \,/\, \psi_{max}; \tag{3}$$

where ψ_{max} = the value of the flux function $\psi = rA$ at the o-point. T and n_0 are thus known only after the solution has been found. We make an initial guess for A; compute ψ_{max}, T, and n_0; compute the corresponding current; invert the curlsquared operator for an improved A; and so iterate, applying an under-relaxation factor of order 0.5 to

*This paper was presented at the Ninth Conference on Numerical Simulation of Plasmas, Northwestern Univ., Evanston, Ill., June 30 - July 2, 1980.

the current. If C_T and C_n are not introduced, convergence is apparently not achieved for all solutions[3].

By integrating the density over volume, the total ion charge is obtained. A representation of the distribution function is obtained by assigning locations and velocities to particles in a manner which yields the correct density and mean azimuthal velocity in each grid cell, within errors associated with finite particle number. The r-z plane is divided into small subcells, and the area-weighted density at each subcell center is used to compute the probability that the subcell contains a particle. An isotropic velocity distribution in the rotating frame is generated, with a user-specified velocity cutoff (for any component) of up to six times $v_{thermal}$.

RIGIDROTOR runs on the NMFECC CDC-7600 (and is available through LIBRIS); the output file is sent to the CRAY-1 where its field and particle initial condition data are used to initialize RINGHYBRID. RINGHYBRID advances the particles along their equilibrium orbits in the time-independent, selfconsistent zero order field. For stability studies of low frequency, nonaxisymmetric modes the code simultaneously advances linearized displacements from these orbits, as well as linearized quasineutral fluid equations for cold ion and electron components, and selfconsistent first order E and B fields, which are fully 3d. When first order E and B are set to zero, the linearized displacements are advanced using forces arising solely from the equilibrium magnetic field and its gradients; they thus serve as diagnostics of the local stability of each orbit.

A variety of field reversed mirror and ion ring equilibria have been obtained; when the equilibrium field and particle initial condition data are used in RINGHYBRID, particle moments remain nearly constant in time. Orbits are, in general, quite complicated, and many (from 10% to most) are stochastic[4]. The complexity of moderate-gyroradius FRM orbits arises from the fact that particles moving along closed field lines may or may not reflect in the high field regions, and furthermore may pass near the field null during their gyratory excursions. Also, the rate of a particle's azimuthal drifting motion depends stongly upon where it lies on its orbit in the r-z plane.

When an orbit is stochastic, the separation between it and any neighboring trajectory increases exponentially in time, with noise superposed. In the nonlinear 2d3v zero order behavior, the only manifestation of orbital stochasticity is an eventual loss of left-right symmetry due to the exponential divergence of "neighboring" mirror image trajectories (due to roundoff effects, they are not perfect mirror

images). This zero order stochastic behavior has been studied both with surface of section plots ($r-\dot{r}$ at midplane) and histories of $|r_1-r_2|$ for mirror image particles. However, the linearized simulation calculates first order currents from the separation of orbits which are displaced from each other by an infinitesimal vector for all time, and in many cases collective behavior can be masked by rapid separation of orbits in the equilibrium field. The stochastic parts of the displacements are random in phase (uncorrelated), and so (if there were an infinitude of particles) they should make no net contribution to any macroscopic quantity such as the current - only the coherent part of the displacement associated with the collective mode should not average to zero. With a relatively small number of particles in each cell, cancellation due to random phases does not occur, and so in practice the current at any given time tends to be dominated by the contribution of the one or several most unstable trajectories. Unless the collective mode being studied has a higher growthrate than the fastest orbit separation rate, the collective behavior is invisible, and the "single-particle modes" dominate (other particles respond to the fields arising from the large offending-particle current).

Attempts to reduce the problem by employing larger numbers of particles were unsuccessful, presumably because cancellation of growing exponentials is impossible; also, as more particles were loaded, some tended to fall on trajectories with even higher associated growthrates. In a few marginal cases the most unstable particles can be removed from the computation artificially, but often too many particles must be excised. Until recently, we have been forced to choose equilibria with low rates of orbit separation, and this has proven to be a significant restriction on the applicability of our program. We have found one moderately thick ion ring equilibrium which does not exhibit rapid stochastic instability, and have examined precessional and kink mode behavior of this system in some detail[5].

Most recently, we have developed a procedure whereby the coherent part of the first order distribution is periodically reconstructed and the random part discarded; the procedure requires an approximate knowledge of the mode structure. As a specific example, we consider the tilting mode of an ion ring; this mode is essentially rigid in nature, the mean axial displacement of particles at any point in the poloidal plane being independent of position in that plane. Thus, every (say) half gyroperiod we compute the mean axial displacement and first order axial velocity of all particles (complex quantities, since the tilt may have any orientation in azimuth), and set the axial displacement and

velocity of each particle equal to these mean values; radial and azimuthal quantities are set to zero. This effectively enforces a rigid tilt on the system, and sets the random part of the displacements to zero. The reconstruction must be done often enough that the coherent part always dominates; the random part must never be allowed to grow from the noise to a large value. When this procedure is applied we are able to observe collective behavior in systems where previously only the stochastic growth was evident. Even though the true mode may not be perfectly rigid, its projection onto a rigid displacement is large enough for the technique to work. In principle one might alter the mode structure variationally to get the peak (true) growthrate.

Future reconstruction schemes might average globally or locally along a fieldline (for flute or ballooning modes), or on a cell-by-cell basis; the latter would eliminate the requirement that we know the poloidal mode structure, but has stiffer statistical requirements. Furthermore, the modes are still restricted to be fluidlike in that the displacements and velocities at each point are single valued. To properly capture all resonant particle effects, the reconstruction must be done in the full phase space, and some knowledge of the mode structure is required. Other possibilities include an orbit averaging scheme (since the modes in question are generally of low frequency, while the noise is often of higher frequencies), and a careful spectral analysis of the data to try to diagnose a small coherent signal in a noisy background.

---

[1]A. Friedman, R.N. Sudan, and J. Denavit, Proc. Eighth Conf. on Numerical Simulation of Plasmas, Paper No. PC-13, Lawrence Livermore Lab. Conf. Proc. No. CONF-780614 (1978); Cornell Univ. Lab. of Plasma Studies Rept. No. 268 (1979, to appear in J. Comp. Phys.).

[2]L. Sparks, J.M. Finn, and R. N. Sudan, Bull. Am. Phys. Soc. 24, 955 (1979).

[3]B. Marder and H. Weitzner, Plasma Phys. 12, 435 (1970).

[4]A. Friedman, "Ergodic Orbits in Particle Simulations of Strong Ion Rings," U. C. Berkeley Electronics Research Lab. Rept. No. M79/41 (1979).

[5]A. Friedman, J. Denavit, and R.N. Sudan, Bull. Am. Phys. Soc. 24, 956 (1979).

Section II
CODE DEVELOPMENT AND MAINTENANCE

A. ES1 CODE

See "Orbit Averaging" in Sec. I, Part D. See "Multibeaming Instabilities" in Sec. I, Part F.

B. EM1 CODE

No special progress.

C. EZOHAR CODE

See "LHD1 Simulations in 2d", Sec. I, Part A.

D. RINGHYBRID CODE

Alex Friedman

Applications of the RINGHYBRID code to exponential rigid rotor equilibria, and a scheme under development which periodically reconstructs the coherent part of the perturbation quantities and discards the random part, are described in the abstract of a paper presented at the Ninth Conference on Numerical Simulation of Plasmas, reproduced elsewhere in this QPR. Here we briefly describe other developments.

A facility for use of the TALLYC postprocessor has been added to the code. Calls to the BZOHAR library routines "timer" and "timend" cause code operation to be interrupted periodically, the program counter value being noted at each interruption. The data are written to a dump file called t<*idrun*>0, and one instructs the TALLYC routine to use this file and the symbol table file as input. Output consists of a table showing how much time is used in each subroutine, and (optionally) a breakdown by code lines of the time used within selected subroutines.

TALLYC and BZOHAR are available from rfilem directory .takeme of userno. 1234. To run TALLYC, type TALLYC t<idrun>0 x5050200 <subroutine names> / t v, where x5050200 is the version of RINGHYBRID's executable file used, containing symbol table information; TALLYC informs the user of the name of the file it produces.

The user can refer to the listing of RINGHYBRID to see how to call "timer" and "timend" in other codes - "9" is the logical unit number, and "itally" and "2000b" are the name and length of a scratch array dimensioned in the cliche "commons". "idrun" and "1" are the header and number of words in the header of the outputfile to be produced by tally.

When this facility is employed in RINGHYBRID, we find that the particle mover consumes the bulk of the cpu time, but that much of the work is concentrated in the gather/scatter (indirect address) parts of the coding which perform field interpolations in scalar mode - the mover itself is vectorized. In principle it is possible to vectorize the gather/scatter also in this code, since the algorithm gathers Re(Br),Im(Br),...,Im(Ez),Br(equilibrium),Bz(equilibrium) = 14 quantities at each of the nine grid points intersected by a particle, and scatters Re(rho),Im(rho),Re(Jr),Im(Jr),...,Im(Jz) = 8 quantities. Thus, minimum vector lengths of 8 are possible, and may be implemented at some point in the future. A greater improvement might be achieved by interleaving the arrays so that all rho,J components at one cell appeared, then all rho,J components at the next cell, and so on, then all B,E,B(equilibrium) components at the first cell, etc. As particles are 3 cells wide in each direction, this would permit a minimum vector length of 24 in the scatter operation (and 42 in the gather). Unfortunately, this change would necessitate a total rewrite of the code, since diagnostics and fieldsolving are based around the present scheme, wherein Re(rho) values at cells 1 through (nz+2)*(nr+2) are stored first, then Im(rho) values, Re(Jr) values, etc.

Also added was a facility for writing a file mode<idrun> which can be interpreted by the postprocessor ZED (after being reformatted by a program called PASTEAF and sent to the CDC-7600).
Spectra computed by ZED based on components of the mean first order displacements (epsilons), or first order magnetic field in a preselected diagnostic cell, are quite clean. This work is in progress; we have enjoyed a collaboration with Bill Nevins in this regard.

A side benefit of the cell-by-cell reconstruction algorithm being implemented is the availablity of a diagnostic revealing the mode structure (spatial dependence of epsilon) in detail. We find that normal modes such as the ion ring tilt are not perfectly rigid, but rather entail displacement peaks at various points in the poloidal plane, typically at largest radius and at the edges of the ring. Some previously-run problems of interest will be re-run with the new diagnostic.

Finally, an extensively revised usage manual for the code is available from filem directory .takeme of usernumber 1234 (on the 7600). New code variables, and revised instructions for running the code, are described. Detailed examples have been added.

E. POLARES: A TWO-DIMENSIONAL R-θ ELECTROSTATIC SIMULATION CODE

Niels F. Otani (Prof. C. K. Birdsall)

We have vectorized the charge-weighting routine and the mover. The code now runs approximately three times faster than before. About 50 μsec are required per particle per timestep for 24 azimuthal Fourier modes — still fairly slow. Vectorization was variously performed with respect to either Fourier mode number or particle index.

A full-dynamics electron-mover scheme is now implemented. This will allow more flexibility in the types of problems we can examine with the code.

Improvements are continuing to be made in the code diagnostics. So far, it is possible to plot any two of r, θ, v_r, and v_θ against one another; also kinetic energy, electric field energy, and total energy history plotting capabilities have been installed. Potential contour plots and mode energy histories are contemplated for the near future.

The difficulty mentioned in the previous QPR concerning the incorrect dipole oscillation period has been corrected. The period observed in the simulations is now in excellent agreement with theory. However, some damping or beating effect of the oscillations has been observed. Also energy conservation is only good to 25% which is unacceptable. These problems are currently under examination.

F. WAVES: A UNIFORM TWO-FLUID ELECTROMAGNETIC DISPERSION RELATION SOLVER

Niels F. Otani (Prof. C. K. Birdsall)

The dispersion relation solver appearing the last QPR has been completely rewritten. The Muller's method solver has been replaced by Newton's method, since all the roots appear to be real. This seems reasonable,

since the only free energy in the system is the difference in the species temperatures; relaxation of this kind of free energy should not be possible in a fluid code.

Operation of the code is fairly straightforward. Initially, a thorough search is made for roots. Initial guesses are made at intervals small compared to the smallest characteristic frequency of the system. The fraction these intervals are of the smallest characteristic frequency is adjustable. An attempt is made to converge each of these guesses to a root. Having found these roots, two options are offered. The user may request the relative values of the wave quantities characteristic of each root. The possibility of degeneracy is allowed for in this option: two orthogonal eigenmodes will be generated for a degenerate root. Alternatively, either the wave number k, or the angle between $\underline{k}$ and $\underline{B}_o$, θ, or both, may be allowed to vary. WAVES will then follow the values of the roots, and plot the resulting dispersion relation.

G. REPORT PREPARATION USING TRIX/RED AND REDPP

Alex Friedman

A system for numbering the equations in reports formatted using this editing system has been developed and made available to us by Art Walstead of LLL (current affiliation UCLA). The abstract prepared by Alex Friedman for the Numerical Simulation Conference (appearing elsewhere in this QPR) was prepared using this system. The RED source file for this abstract, and a COSMOS deck which sends test copies to the local Versatec printer, are available from filem directory .takeme of usernumber 1234 - they are called "simconf" and "swapsim" respectively (refer to QPR's II,III of 1979 for details on generating typeset output, and for other notes).

Note that equations are defined (using macro "eqt") before they are employed (using macro "eqn" - the last argument is the number of lines to be set aside for the equation). Macros, and basic page layout, are defined at the top of the source file. Note also the usefulness of the "quotient" facility "qt" to define frequently occurring or complicated expressions.

Finally, it is possible to prefix "chapter" numbers to the equation numbers to get, for example, (5.13) instad of just (13). To do this, change "ns(dum,<num>)" to "ns(dum,<5.num>)" in the macro definition for eqn.

One drawback of this system is that line numbers as they appear when the source is listed on the Versatec do not agree with those evident when using TRIX; the latter are correct, and so the user must mentally alter the listed numbers by one when referring to a Versatec listing. (One of the line throws is not recognized by the Versatec - there should be three "trix" commands in a row near

lines 43-44, and so for line numbers in the bulk of the text after this point one has to add one to the number the Versatec prints out.)

Another example of this type of formatting is an excerpt from Walstead's thesis, called "art's.memo" and also available from the filem directory .takeme. The user is encouraged to format and print this section as well, since it provides a more complete illustration of the capabilities of the system.

H. FREX

H. Stephen Au-Yeung

FREX has been updated on June 9, 1980. The new version has the following changes:

(1) The output file name now begins with "f3" instead of "f0" to match the TV80LIB new file naming convention.

(2) The size of the output file will now be expanded if necessary; therefore the SIZE command is not required for large files anymore.

Section III

SUMMARY OF REPORTS, TALKS, PUBLICATIONS, VISITORS

Abstracts for two papers presented at the Sherwood Fusion Theory Meeting, April 23-25 were in the previous QPR.

Four papers were presented at the Ninth Conference on Numerical Simulation of Plasmas at Northwestern University, Evanston IL, June 30 - July 2, as follows:

Paper	
PB-6	V. Thomas and C. K. Birdsall, "Plasma Hybrid Oscillations as Affected by Aliasing" (much as in prior QPR's)
OB-3	Alex Friedman, "Field Reversed Equilibria, Intrinsic Stochasticity, and Collective Stability" (See Sec. I, Part H for abstract)
OB-5	V. Thomas and B. I. Cohen, "Orbit Averaging in an Electrostatic Code" (much as in prior QPR's)
PC-6	Jin-Soo Kim and C. K. Birdsall, "Magnetized Multi-Ring Instabilities" (much as in this QPR)

The following paper was published:

C. K. Birdsall and Neil Maron, "Plasma Self-Heating and Saturation Due to Numerical Instabilities", J. Comp. Phys. 36, pp. 1-19, June 1980.

We were visited by M. J. Gerver for the week of May 12.

DISTRIBUTION LIST 1

Department of Energy

Manley, Nelson, Sadowsky, Dobrott

Department of Navy

Condell, Roberson, Florance

Austin Research Associates

Drummond, Moore

Bell Telephone Laboratories

Hasegawa

Calif. Institute of Technology

Liewer

Calif. State Polytech. Univ.

Rathman

Columbia University

Chu

Cornell University

Mankofsky

Electrical Power Research Inst.

Gough, Scott

General Atomic Company

Helton, Lee

Georgia Institute of Technology

Bateman

Hascom Air Force Base

Rubin

IBM Corporation

Gazdag

JAYCOR

Klein, Tumolillo, Hobbs

Kirtland Air Force Base

Pettus

Los Alamos Scientific Laboratory

Barnes, Burnett, Forslund, Gitomer, Hewett, Lindemuth, Mason, Neilson, Oliphant, Sgro

Lawrence Berkeley Laboratory

Cooper, Kaufman, Kim, Kunkel, Pyle, Sternlieb

Lawrence Livermore National Laboratory

Albritton, Anderson, Brengle, Briggs, Bruijnes, Byers, Chambers, Cohen, Drupke, Estabrook, Fawley, Finan, Fries, Fuss, Harte, Killeen, Kruer, Langdon, Lasinski, Lee, Maron, Matsuda, Max, McNamara, Mirin, Nevins, Nielson, Smith, Tull

Mass. Institute of Technology

Berman, Bers, Gerver, Kulp, Palevsky

Mission Research Corporation

Godfrey

U. S. Naval Research Laboratory

Boris, Drobot, Craig, Haber, Orens, Vomvoridis, Winsor

Northwestern University

Crystal, Denavit

New York University

Grad, Weitzner

Oak Ridge National Laboratory

Dory, Meier, Mook

Princeton Plasma Physics Laboratory

Chen, Cheng, Lee, Okuda, Tajima, Tang

Princeton University

Graydon

DISTRIBUTION LIST 2

Science Applications, Inc.

McBride, Siambis, Wagner

Sandia Laboratories, Albuquerque

Freeman, Poukey, Quintenz

Sandia Laboratories, Livermore

Marx

Massachusetts

Johnston

Stanford University

Buneman

University of Arizona

Morse

Univ. of California, Berkeley

Arons, AuYeung, Birdsall, Chen, Chorin, Friedman, Grisham, Harned, Hudson, Keith, Lichtenberg, Lieberman, McKee, Otani, Potter, Thomas

University of California, Davis

DeGroot, Woo

University of California, Irvine

Rynn

University of Calif., Los Angeles

Dawson, Decyk, Huff, Lin

University of Iowa

Joyce, Knorr, Nicholson

University of Maryland

Guillory, Rowland, Winske

University of Pittsburgh

Zabusky

University of Texas

Horton, MacMahon

University of Wisconsin

Shohet

Culham Laboratory

Eastwood,, Roberts

University of Reading

Hockney

Ecole Polytechnique / Centre de Polytech.

Adam

Bhabha Atomic Research Centre

Aiyer, Gioel

Isreal

Gell

Tel-Aviv University

Cuperman

Kyoto University

Abe

Nagoya University

Kamimura

Max Planck Inst. fur Plasmaphysik

Biskamp, Kraft

Universitat Kaiserslautern

Wick